7. Ito M, Masumi A, Mochida K, Kukihara H, Moriishi K, et al. (2010) Peripheral B cells may serve as a reservoir for persistent hepatitis C virus infection. J Innate Immun 2: 607–617.
8. Pal S, Sullivan DG, Kim S, Lai KK, Kae J, et al. (2006) Productive replication of hepatitis C virus in perihepatic lymph nodes in vivo: implications of HCV lymphotropism. Gastroenterology 130: 1107–1116.
9. Karavattathayyil SJ, Kalkeri G, Liu HJ, Gaglio P, Garry RF, et al. (2000) Detection of hepatitis C virus RNA sequences in B-cell non-Hodgkin lymphoma. Am J Clin Pathol 113: 391–398.
10. Ferri C, Zignego AL (2000) Relation between infection and autoimmunity in mixed cryoglobulinemia. Curr Opin Rheumatol 12: 53–60.
11. Mariette X (1999) Lymphomas in patients with Sjogren's syndrome: review of the literature and physiopathologic hypothesis. Leuk Lymphoma 33: 93–99.
12. Mizukawa Y, Shiohara T (2000) Virus-induced immune dysregulation as a triggering factor for the development of drug rashes and autoimmune diseases: with emphasis on EB virus, human herpesvirus 6 and hepatitis C virus. J Dermatol Sci 22: 169–180.
13. Kondo Y, Ueno Y, Kakazu E, Kobayashi K, Shiina M, et al. (2011) Lymphotropic HCV strain can infect human primary naive CD4+ cells and affect their proliferation and IFN-gamma secretion activity. J Gastroenterol 46: 232–241.
14. MacParland SA, Pham TN, Gujar SA, Michalak TI (2006) De novo infection and propagation of wild-type Hepatitis C virus in human T lymphocytes in vitro. J Gen Virol 87: 3577–3586.
15. Hu Y, Shahidi A, Park S, Guilfoyle D, Hirshfield I (2003) Detection of extrahepatic hepatitis C virus replication by a novel, highly sensitive, single-tube nested polymerase chain reaction. Am J Clin Pathol 119: 95–100.
16. Bassiouny DA, Shaker O (2011) Role of interleukin-17 in the pathogenesis of vitiligo. Clinical and experimental dermatology 36: 292–297.
17. Horie I, Abiru N, Saitoh O, Ichikawa T, Iwakura Y, et al. (2011) Distinct role of T helper Type 17 immune response for Graves' hyperthyroidism in mice with different genetic backgrounds. Autoimmunity 44: 159–165.
18. Horie I, Abiru N, Sakamoto H, Iwakura Y, Nagayama Y (2011) Induction of autoimmune thyroiditis by depletion of CD4+CD25+ regulatory T cells in thyroiditis-resistant IL-17, but not interferon-gamma receptor, knockout nonobese diabetic-H2h4 mice. Endocrinology 152: 4448–4454.
19. Zhao L, Tang Y, You Z, Wang Q, Liang S, et al. (2011) Interleukin-17 contributes to the pathogenesis of autoimmune hepatitis through inducing hepatic interleukin-6 expression. PLoS One 6: e18909.
20. Ivanov, II, McKenzie BS, Zhou L, Tadokoro CE, Lepelley A, et al. (2006) The orphan nuclear receptor RORgammat directs the differentiation program of proinflammatory IL-17+ T helper cells. Cell 126: 1121–1133.
21. Harris TJ, Grosso JF, Yen HR, Xin H, Kortylewski M, et al. (2007) Cutting edge: An in vivo requirement for STAT3 signaling in TH17 development and TH17-dependent autoimmunity. Journal of immunology 179: 4313–4317.
22. Seddighzadeh M, Gonzalez A, Ding B, Ferreiro-Iglesias A, Gomez-Reino JJ, et al. (2012) Variants Within STAT Genes Reveal Association with Anticitrullinated Protein Antibody-negative Rheumatoid Arthritis in 2 European Populations. The Journal of rheumatology 39: 1509–1516.
23. Yu CR, Lee YS, Mahdi RM, Surendran N, Egwuagu CE (2012) Therapeutic targeting of STAT3 (signal transducers and activators of transcription 3) pathway inhibits experimental autoimmune uveitis. PLoS One 7: e29742.
24. Machida K, Cheng KT, Sung VM, Levine AM, Foung S, et al. (2006) Hepatitis C virus induces toll-like receptor 4 expression, leading to enhanced production of beta interferon and interleukin-6. J Virol 80: 866–874.
25. Korn T, Bettelli E, Oukka M, Kuchroo VK (2009) IL-17 and Th17 Cells. Annual review of immunology 27: 485–517.
26. Kondo Y, Iwata T, Haga T, Kimura O, Ninomiya M, et al. (2013) Eradication of hepatitis C virus could improve immunological status and pyoderma gangrenosum-like lesions. Hepatology research: the official journal of the Japan Society of Hepatology.
27. Negro F, Krawczynski K, Quadri R, Rubbia-Brandt L, Mondelli M, et al. (1999) Detection of genomic- and minus-strand of hepatitis C virus RNA in the liver of chronic hepatitis C patients by strand-specific semiquantitative reverse-transcriptase polymerase chain reaction. Hepatology 29: 536–542.
28. Hu Y, Shahidi A, Park S, Guilfoyle D, Hirshfield I (2003) Detection of extrahepatic hepatitis C virus replication by a novel, highly sensitive, single-tube nested polymerase chain reaction. American journal of clinical pathology 119: 95–100.
29. Sung VM, Shimodaira S, Doughty AL, Picchio GR, Can H, et al. (2003) Establishment of B-cell lymphoma cell lines persistently infected with hepatitis C virus in vivo and in vitro: the apoptotic effects of virus infection. J Virol 77: 2134–2146.
30. Tuomela S, Salo V, Tripathi SK, Chen Z, Laurila K, et al. (2012) Identification of early gene expression changes during human Th17 cell differentiation. Blood 119: e151–160.
31. Takeuchi K, Kubo Y, Boonmar S, Watanabe Y, Katayama T, et al. (1990) Nucleotide sequence of core and envelope genes of the hepatitis C virus genome derived directly from human healthy carriers. Nucleic acids research 18: 4626.
32. Zhou J, Yu Z, Zhao S, Hu L, Zheng J, et al. (2009) Lentivirus-based DsRed-2-transfected pancreatic cancer cells for deep in vivo imaging of metastatic disease. The Journal of surgical research 157: 63–70.
33. Shiokawa M, Takahashi T, Murakami A, Kita S, Ito M, et al. (2010) In vivo assay of human NK-dependent ADCC using NOD/SCID/gammac(null) (NOG) mice. Biochemical and biophysical research communications 399: 733–737.
34. Chen XQ, Yu YC, Deng HH, Sun JZ, Dai Z, et al. (2010) Plasma IL-17A is increased in new-onset SLE patients and associated with disease activity. J Clin Immunol 30: 221–225.
35. Pan HF, Leng RX, Feng CC, Li XP, Chen GM, et al. (2012) Expression profiles of Th17 pathway related genes in human systemic lupus erythematosus. Mol Biol Rep.
36. Hu Y, Li H, Zhang L, Shan B, Xu X, et al. (2012) Elevated profiles of Th22 cells and correlations with Th17 cells in patients with immune thrombocytopenia. Hum Immunol 73: 629–635.
37. Bergqvist A, Sundstrom S, Dimberg LY, Gylfe E, Masucci MG (2003) The hepatitis C virus core protein modulates T cell responses by inducing spontaneous and altering T-cell receptor-triggered Ca2+ oscillations. J Biol Chem 278: 18877–18883.
38. Dominguez-Villar M, Munoz-Suano A, Anaya-Baz B, Aguilar S, Novalbos JP, et al. (2007) Hepatitis C virus core protein up-regulates anergy-related genes and a new set of genes, which affects T cell homeostasis. J Leukoc Biol 82: 1301–1310.
39. Kogure T, Lin WL, Yan IK, Braconi C, Patel T (2011) Intercellular nanovesicle-mediated microRNA transfer: a mechanism of environmental modulation of hepatocellular cancer cell growth. Hepatology 54: 1237–1248.
40. Tamai K, Shiina M, Tanaka N, Nakano T, Yamamoto A, et al. (2012) Regulation of hepatitis C virus secretion by the Hrs-dependent exosomal pathway. Virology 422: 377–385.
41. Stump KL, Lu LD, Dobrzanski P, Serdikoff C, Gingrich DE, et al. (2011) A highly selective, orally active inhibitor of Janus kinase 2, CEP-33779, ablates disease in two mouse models of rheumatoid arthritis. Arthritis research & therapy 13: R68.
42. Zhang X, Yue P, Page BD, Li T, Zhao W, et al. (2012) Orally bioavailable small-molecule inhibitor of transcription factor Stat3 regresses human breast and lung cancer xenografts. Proc Natl Acad Sci U S A 109: 9623–9628.

JVI
Journals.ASM.org

Hepatitis C Virus Entry Is Impaired by Claudin-1 Downregulation in Diacylglycerol Acyltransferase-1-Deficient Cells

Pil Soo Sung,[a] Asako Murayama,[b] Wonseok Kang,[a] Myung-Sun Kim,[c] Seung Kew Yoon,[d] Masayoshi Fukasawa,[e] Masuo Kondoh,[f] Jin-Soo Kim,[g] Hyongbum Kim,[c] Takanobu Kato,[b] Eui-Cheol Shin[a]

Laboratory of Immunology and Infectious Diseases, Graduate School of Medical Science and Engineering, KAIST, Daejeon, Republic of Korea[a]; Department of Virology II, National Institute of Infectious Diseases, Tokyo, Japan[b]; Graduate School of Biomedical Science and Engineering, College of Medicine, Hanyang University, Seoul, Republic of Korea[c]; Department of Internal Medicine, College of Medicine, The Catholic University of Korea, Seoul, Republic of Korea[d]; Department of Biochemistry and Cell Biology, National Institute of Infectious Diseases, Tokyo, Japan[e]; Laboratory of Bio-Functional Molecular Chemistry, Graduate School of Pharmaceutical Sciences, Osaka University, Osaka, Japan[f]; Center for Genome Engineering, Institute for Basic Science, and Department of Chemistry, Seoul National University, Seoul, Republic of Korea[g]

ABSTRACT

Diacylglycerol acyltransferase-1 (DGAT1) is involved in the assembly of hepatitis C virus (HCV) by facilitating the trafficking of the HCV core protein to the lipid droplet. Here, we abrogated DGAT1 expression in Huh-7.5 cells by using either the transcription activator-like effector nuclease (TALEN) or lentivirus vector short hairpin RNA (shRNA) and achieved complete long-term silencing of DGAT1. HCV entry was severely impaired in DGAT1-silenced Huh-7.5 cell lines, which showed markedly diminished claudin-1 (CLDN1) expression. In DGAT1-silenced cell lines, the forced expression of CLDN1 restored HCV entry, implying that the downregulation of CLDN1 is a critical factor underlying defective HCV entry. The expression of the gene coding for hepatocyte nuclear factor 4α (HNF4α) and other hepatocyte-specific genes was also reduced in DGAT1-silenced cell lines. After *DGAT1* gene rescue, CLDN1 expression was preserved, and HCV entry was restored. Strikingly, after DGAT1 silencing, CLDN1 expression and HCV entry were also restored by low-dose palmitic acid treatment, indicating that the downregulation of CLDN1 was associated with altered fatty acid homeostasis in the absence of DGAT1. Our findings provide novel insight into the role of DGAT1 in the life cycle of HCV.

IMPORTANCE

In this study, we report the novel effect of complete silencing of DGAT1 on the entry of HCV. DGAT1 was recently reported as a host factor of HCV, involved in the assembly of HCV by facilitating the trafficking of the HCV core protein to lipid droplets. We achieved complete and long-term silencing of DGAT1 by either TALEN or repeated transduction of lentivirus shRNA. We found that HCV entry was severely impaired in DGAT1-silenced cell lines. The impairment of HCV entry was caused by CLDN1 downregulation, and the expression of HNF4α and other hepatocyte-specific genes was also downregulated in DGAT1-silenced cell lines. Our results suggest new roles of DGAT1 in human liver-derived cells: maintaining intracellular lipid homeostasis and affecting HCV entry by modulating CLDN1 expression.

Hepatitis C virus (HCV) infection poses a major threat to human health, with a prevalence of more than 160 million people worldwide (1). In addition to a combination regimen of pegylated interferon alpha (IFN-α) and ribavirin, drugs acting directly on HCV have now been developed, although these direct-acting antivirals may prompt the emergence of resistant strains (2, 3). Our increasing understanding of the HCV-host interactions is allowing novel therapeutic approaches to be developed that modulate host factors that are required for viral entry, replication, and egress; these factors may have a higher genetic barrier to viral resistance (4).

Diacylglycerol acyltransferase-1 (DGAT1) is one of two known DGAT enzymes catalyzing the final step in triglyceride biosynthesis (5, 6). The expression of DGAT1 and its physiologic role differ in humans and mice. In mice, DGAT1 is expressed in many organs, including the skeletal muscle, heart, and intestines, but it is barely expressed in the liver (5). Because DGAT1-deficient mice are resistant to diet-induced obesity (7), pharmacological DGAT1 inhibitors are being developed for the treatment of metabolic diseases (8). In contrast to mice, human DGAT1 is mainly expressed in the small intestine and liver (9). Human DGAT1 reesterifies partial glycerides to triglycerides using exogenous fatty acids. In addition, intracellular lipid homeostasis is dysregulated in human hepatocytes in the absence of DGAT1 (10).

As a host factor interacting with HCV, DGAT1 has drawn attention for its role in trafficking the HCV core protein to lipid droplets (11). In addition, the same study reported that treatment with a DGAT1 inhibitor blocked the association of the HCV core protein with lipid droplets and decreased the production of infectious HCV virions (11). Further research has demonstrated that DGAT1 is involved in the localization of the HCV NS5A protein to lipid droplets and promotes NS5A interaction with the HCV core protein (12). However, in these reports, DGAT1 inhibitors were

Received 17 May 2014 Accepted 29 May 2014
Published ahead of print 4 June 2014
Editor: M. S. Diamond
Address correspondence to Eui-Cheol Shin, ecshin@kaist.ac.kr.
Supplemental material for this article may be found at http://dx.doi.org/10.1128/JVI.01428-14.

doi:10.1128/JVI.01428-14

mainly used to block DGAT1 activity, and the observation was limited to as late as 72 h after treatment with DGAT1 inhibitors.

In the present study, we investigated the effects of complete, long-term silencing of DGAT1 on the whole life cycle of HCV. We established DGAT1 knockdown cell lines and a DGAT1 knockout (KO) cell line and observed that the entry of HCV into DGAT1-silenced cells was impaired. Furthermore, we identified the underlying mechanism of defective HCV entry into these cell lines.

MATERIALS AND METHODS

Cell culture. Huh-7.5 cells (Apath, LLC, Brooklyn, NY) (13), HepG2 cells (ATCC, Manassas, VA), Caco-2 cells (ATCC, Manassas, VA), and 293TN cells (System Biosciences, Mountain View, CA) were maintained at 37°C with 5% CO_2 in Dulbecco's modified Eagle's medium supplemented with 10% fetal bovine serum (WelGENE, Daegu, South Korea), 4.5 g/liter glucose, L-glutamine, and 1% penicillin-streptomycin (Invitrogen, Carlsbad, CA). Short hairpin RNA (shRNA)-transduced cells were maintained in complete medium containing 1 μg/ml puromycin (Sigma-Aldrich, St. Louis, MO), and shRNA-resistant DGAT1-transfected cells were cultured in complete medium that was supplemented with 1 μg/ml puromycin and 1 mg/ml G418 (A.G. Scientific, San Diego, CA). All of the transfections were performed using Lipofectamine 2000 (Invitrogen, Carlsbad, CA).

Generation and infection of JFH-1 HCVcc. The Japanese fulminant hepatitis 1 (JFH-1) strain (genotype 2a) (14) of cell-culture-derived HCV (HCVcc) (15–17) was generated and propagated as previously described (18). For the titration of HCV infectivity, a colorimetric focus-forming assay was performed as previously described (19). Cell cultures were inoculated with JFH-1 HCVcc at a multiplicity of infection (MOI) of 0.1 to 0.5.

HCVpp entry assay. For the evaluation of HCV entry, HCV pseudoparticles (HCVpp) with E1 and E2 glycoproteins of various HCV genotypes (H77, genotype 1a; TH, genotype 1b; JFH-1, genotype 2a; and J6CF, genotype 2a) were generated, and cell cultures were inoculated as previously described (20, 21). Virus pseudoparticles with vesicular stomatitis virus glycoproteins (VSV-G) were used as positive controls.

Preparation and transduction of shRNA-DGAT1-expressing lentiviruses. Three bacterial glycerol stocks with lentiviral shRNA constructs expressing validated sequences of DGAT1 (shRNA-DGAT1) and one stock with lentiviral constructs expressing validated sequences of DGA2 (shRNA-DGAT2) were purchased from Sigma-Aldrich. The sequences that are recognized by these shRNAs are presented in Fig. S1 in the supplemental material. A control shRNA vector (shRNA-control) encoding a scrambled sequence was also prepared. Lentiviral vectors comprising VSV-G plasmid, gag-pol plasmid, and a MISSION shRNA plasmid were transfected into 293TN cells using Lipofectamine 2000 (Invitrogen). After 48 h of transfection, lentiviral particles were harvested, passed through a 0.45-μm-pore syringe filter, concentrated with WelProt virus concentration reagent (WelGENE), and stored at −70°C. To maximize transduction efficiency, cells were repeatedly transduced with concentrated lentivirus. After 48 h of transduction, the cells were treated with 1 μg/ml puromycin and expanded over 3 to 6 weeks in puromycin-containing selection medium until they showed a stable phenotype. For the forced expression of CLDN1, shRNA-DGAT1-transduced cell lines were transfected with a plasmid-encoding *CLDN1* gene cloned from Huh-7 cells and regulated by an EF-1α promoter.

Generation of DGAT1-KO cell line using TALEN. The target sequence of the *DGAT1*-targeting transcription activator-like effector nuclease (TALEN) was TGCCATCGCCTGCAGGATTC (left)-TTTATTCA GCTCT (spacer)-GACAGTGGCTTCAGCAACTA (right). The plasmid encoding *DGAT1*-targeting TALEN was prepared as recently described (22) and provided by Toolgen, Seoul, Republic of Korea (http://www.talenlibrary.net/) (order no. H157465). Huh-7.5 cells were cotransfected with a total of 8 μg DNA comprising 2 μg of plasmid encoding one member of the *DGAT1*-targeting TALEN, 2 μg of plasmid encoding another member of the TALENs, and 4 μg of the reporter encoding H-$2K^k$ (23) via electroporation using the Invitrogen Neon transfection system (at a voltage of 1,100 V for 30 ms, using a 100-ml tip and one pulse). The transfected cells were cultured for 1 day at 37°C and for 2 days at 30°C (cold shock) (24) and subjected to magnetic separation as previously described (23). Briefly, trypsinized cells were mixed with magnetic bead-conjugated antibodies against H-$2K^k$ (MACSelect K^k microbeads; Miltenyi Biotech, Germany) and incubated for 20 min at 4°C. Labeled cells were separated using a MACS LS column (Miltenyi Biotech). The DGAT1 mutant cells that were enriched by this magnetic separation were plated into 96-well plates at a density of 0.25 cell/well. Two weeks after plating, only single-cell-derived colonies of a circular shape were manually selected under a microscope. Genomic DNA was isolated using the DNeasy blood and tissue kit (Qiagen, Valencia, CA). We analyzed 62 single-cell-derived colonies using the T7E1 enzyme digestion assay, which selectively detects heteroduplex DNA that results from gene editing by TALEN. We also analyzed these colonies by sequencing. The region of the *DGAT1* gene containing the TALEN target site was amplified by nested PCR (primer sequence, 1st PCR, forward, 5′-CAAGCTCCATGTAGGTCCAG-3′, and reverse, 5′-CTCTCCTGGGATCCAATG-3′; 2nd PCR, forward, 5′-TCT GACCCTGACATGCTCGT-3′, and reverse, 5′-CCAATGGGAAGCAGC AAGTA-3′), cloned into the T-Blunt vector, and sequenced.

Flow cytometry. For the detection of HCV receptors on the cell surface, the following antibodies were used: phycoerythrin (PE)-conjugated mouse monoclonal anti-CD81 IgG1 (clone JS-81; BD Biosciences, San Jose, CA), mouse monoclonal anti-CLDN1 (clone 7A5; developed by DNA immunization of the CLDN1 expression construct), rabbit polyclonal anti-SR-B1 (clone H-180; BD Biosciences), and rabbit polyclonal anti-occludin (anti-OCLN) (Sigma-Aldrich). For the staining of OCLN, the cells were fixed and permeabilized using the Foxp3 staining kit (eBioscience, San Diego, CA). PE-conjugated goat anti-rabbit IgG (Santa Cruz Biotechnology, Inc., Santa Cruz, CA) was used as a secondary antibody for the SR-B1 and OCLN staining. For the intracellular staining of DGAT1, mouse monoclonal anti-DGAT1 IgG1 (A-5; Santa Cruz Biotechnology, Inc.) was used as a primary antibody, and allophycocyanin (APC)-conjugated anti-mouse IgG (BD Biosciences) was used as a secondary antibody. For the intracellular staining of the HCV core protein, mouse monoclonal anti-HCV core IgG1 (clone C7-50; Thermo Scientific/Affinity BioReagents, Rockford, IL) was used as a primary antibody, and fluorescein isothiocyanate (FITC)-conjugated anti-mouse IgG1 (clone A85-1; BD Biosciences) was used as a secondary antibody. For the intracellular staining, the cells were fixed and permeabilized using the Foxp3 staining kit (eBioscience) and then stained with the primary antibody for 20 min at 4°C. After a washing step with permeabilization buffer (eBioscience), the cells were stained with the appropriate secondary antibodies. The LSR II instrument (BD Biosciences) was used for the flow cytometry. The FlowJo software (TreeStar, Ashland, OR) was used for data analysis.

Immunoblots. Cell lysates were prepared, and 20 μg of each lysate was loaded onto SDS-PAGE gels and analyzed by immunoblotting. The antibodies that were used for the immunoblots were as follows: mouse monoclonal anti-DGAT1 IgG1 (clone A-5; Santa Cruz Biotechnology, Inc.), rabbit polyclonal anti-DGAT1 (H-255; Santa Cruz Biotechnology, Inc.), rabbit polyclonal anti-DGAT2 (Sigma-Aldrich), rabbit polyclonal anti-CLDN1 (Abcam, Cambridge, United Kingdom), rabbit polyclonal anti-hepatocyte nuclear factor 4α (anti-HNF4α) (H-171; Santa Cruz Biotechnology, Inc.), and mouse monoclonal anti-tubulin (clone B-5-1-2; Sigma-Aldrich). Following the blotting, the membrane was incubated with primary antibodies (diluted at 1:200 to 1:1,000) overnight at 4°C or for 1 h at room temperature. The signal was detected using the horseradish peroxidase-conjugated secondary antibody (Jackson Immuno Research Laboratories, West Grove, PA) with enhanced chemiluminescence reagents (GE Healthcare/Amersham, Buckinghamshire, United Kingdom).

Confocal microscopy. The antibodies that were used for the confocal microscopy imaging were as follows: mouse monoclonal anti-claudin-1 (anti-CLDN1) (clone 1C5-D9; Abcam), rabbit polyclonal anti-occludin

(Invitrogen), Cy3-conjugated goat anti-mouse IgG (Jackson Immuno Research Laboratories, West Grove, PA), and Alexa Fluor 488-conjugated donkey anti-rabbit IgG (BioLegend, San Diego, CA). The cells were fixed with 4% paraformaldehyde for 20 min and permeabilized with 0.5% (vol/vol) Triton X-100 for 10 min. The slides were incubated with primary antibodies (diluted at 1:100) for 3 h at room temperature. After being washed with phosphate-buffered saline three times, they were incubated with secondary antibodies (diluted at 1:1,000). Following the addition of mounting solution, images were acquired using an LSM-510 confocal laser-scanning microscope (Carl Zeiss, Jena, Germany).

Intracellular lipid droplet quantification. Cells were fixed with 2% paraformaldehyde for 20 min on slides and permeabilized with 0.5% (vol/vol) Triton X-100 for 10 min. The slides were incubated in phosphate-buffered saline (PBS) containing 10 μM BODIPY (boron-dipyrromethene) lipid probe 493/503 (Invitrogen) for 1 h at room temperature. After the addition of mounting solution, images were acquired using an LSM-510 confocal laser-scanning microscope (Carl Zeiss). For the flow cytometry analysis, control and DGAT1-silenced cells were pelleted and resuspended in fluorescence-activated cell sorter (FACS) buffer (PBS with 2% fetal bovine serum [FBS], 2 mM EDTA). Then, cells were fixed and permeabilized using a Foxp3 staining kit (eBioscience). After permeabilization, the cells were resuspended with FACS buffer containing 10 μM BODIPY lipid probe 493/503 and incubated for 30 min in the dark. Next, the cells were washed in FACS buffer, pelleted, and resuspended in FACS buffer. Up to 50,000 events were detected using the LSR II instrument (BD Biosciences) for flow cytometry. FlowJo software (TreeStar) was used for the data analysis.

RNA extraction, cDNA synthesis, and real-time qPCR. Total RNA isolation, cDNA synthesis, and TaqMan real-time quantitative PCR (qPCR) were performed as previously described (18). In brief, total RNA was isolated with the RNeasy minikit (Qiagen), and cDNA was synthesized using an Applied Biosystems high-capacity cDNA synthesis kit (Applied Biosystems, Foster City, CA). TaqMan gene expression assays (Applied Biosystems) were used to determine the mRNA levels of the target genes. For the titration of intracellular HCV RNA copies, the sequences of the primers and probes that were used are as follows (25): forward, CGG GAG AGC CAT AGT GG-3; reverse, AGT ACC ACA AGG CCT TTC G; and probe, 6-carboxyfluorescein (FAM)-CTG CGG AAC CGG TGA GTA CAC-6-carboxytetramethylrhodamine (TAMRA). The results were standardized to an endogenous control, β-actin.

Palmitic acid treatment and cell culture. Cells were incubated in medium containing 10% charcoal-stripped fetal bovine serum (WelGENE) that was supplemented with 50 μM palmitic acid (Sigma-Aldrich) or dimethyl sulfoxide (DMSO) in complexes with 1% bovine serum albumin (BSA). The medium was changed every 2 days for the continuous treatment.

Cell proliferation and viability assay. The cell proliferation activities were assessed using the BD Biosciences apoptosis, DNA damage, and cell proliferation kit according to the manufacturer's protocol. A 1 mM concentration of bromodeoxyuridine (BrdU) was incorporated into the control and DGAT1-silenced cell lines for 3 h. For the flow cytometry analysis, control and DGAT1-silenced cells were pelleted and resuspended in FACS buffer. Then, the cells were fixed and permeabilized, treated with DNase, stained with peridinin chlorophyll protein (PerCP)-Cy5.5-conjugated mouse anti-BrdU (BD Biosciences), and incubated for 30 min in the dark. Next, cells were washed in FACS buffer, pelleted, and resuspended in FACS buffer. Up to 50,000 events were detected using the LSR II instrument (BD Biosciences). FlowJo software (TreeStar) was used for the data analysis. For the cell viability assay, the cells were fixed and permeabilized, stained with PE-conjugated mouse anti-cleaved poly(ADP-ribose) polymerase (PARP) (Asp214) antibody, and incubated for 30 min in the dark. Data were obtained using the LSR II instrument (BD Biosciences).

ChIP. Chromatin immunoprecipitation (ChIP) assays were performed according to the manufacturer's instructions (Pierce agarose ChIP kit; Pierce, Rockford, IL). Approximately 1×10^6 cells were used for each immunoprecipitation. Whole-cell lysates were immunoprecipitated using 1 μg of rabbit anti-HNF4α (H171) (Santa Cruz Biotechnology, Inc.) or IgG. Real-time qPCR was used to amplify the region near the HNF4α binding site in the promoter of the *CLDN1* gene (26, 27). Reactions were performed in triplicate in three independent experiments, and the means were normalized to 1% of the chromatin input.

Statistical analyses. Data are presented as means ± standard errors of the means (SEM). Unpaired *t* tests or two-tailed Mann-Whitney U tests were performed. All of the statistical analyses were conducted using GraphPad Prism version 5.01 (GraphPad Software, San Diego, CA). A P value of <0.05 was considered statistically significant.

RESULTS

Establishment of DGAT1-silenced Huh-7.5 cell lines using either TALEN or lentivirus vector shRNA. To identify the effects of complete, long-term silencing of DGAT1 on the whole life cycle of HCV in Huh-7.5 cells, we knocked down DGAT1 expression by lentivirus vector shRNA transduction or knocked out the *DGAT1* gene using a pair of TALENs in these cells. Three stable cell lines (shRNA-DGAT1-1666, shRNA-DGAT1-1183, and shRNA-DGAT1-1402) were established by the repeated transduction of three different lentiviruses carrying shRNA (see Fig. S1 in the supplemental material) and expanded in puromycin-containing selection medium for more than 2 months. For the more complete silencing of DGAT1 without residual expression, we established a *DGAT1*-knockout cell line (DGAT1-TALEN) using TALENs. To isolate cells in which the TALEN-knocked out DGAT1, we transfected Huh-7.5 cells with plasmids encoding a pair of *DGAT1*-targeting TALENs in combination with a reporter plasmid. The reporter plasmid expressed H-2K^k when a pair of *DGAT1*-targeting TALENs functioned successfully in the transfected cells. After transfection, we selected H-2K^k-expressing cells using magnetic bead-conjugated anti-H-2K^k antibodies. We analyzed 62 single-cell-derived colonies using a T7E1 enzyme digestion assay, which selectively detects heteroduplex DNA resulting from gene editing by TALEN (Fig. 1A), and then we chose a *DGAT1*-knockout cell line harboring a shifted open reading frame or premature stop codon in the *DGAT1* gene (Fig. 1B). In the cell lines with DGAT1 that was silenced by either shRNA or TALEN, we verified the loss of DGAT1 expression at both the mRNA and protein levels. The expression of DGAT1 mRNA in the shRNA-DGAT1-transduced cell lines was less than 20% of that in a control cell line (shRNA-control), and DGAT1 mRNA was not detected in the DGAT1-TALEN cell line (Fig. 1C). The DGAT1 protein was deficient in all of the DGAT1-silenced cell lines (Fig. 1D).

We compared several basic characteristics of the DGAT1-silenced cell lines with those of the control cell line. For example, triglyceride-rich intracellular lipid droplets were barely detectable in the DGAT1-silenced cell lines, whereas they were abundant in the control cell line (Fig. 1E). Cell proliferation and apoptosis were also analyzed by BrdU incorporation and cleaved PARP staining, respectively. Cell proliferation rates were higher in the DGAT1-silenced cell lines than in the control cell line, whereas apoptotic death was not altered (data not shown).

HCV entry is impaired in DGAT1-silenced Huh-7.5 cell lines. To identify the effects of DGAT1 silencing on the whole life cycle of HCV, we inoculated DGAT1-silenced Huh-7.5 cell lines with JFH-1 cell culture-produced HCV (HCVcc) and measured infectious virions in the culture supernatants. In accordance with the role of DGAT1 in the assembly of HCV, infectious virions were not detected in the culture supernatants of the DGAT1-silenced

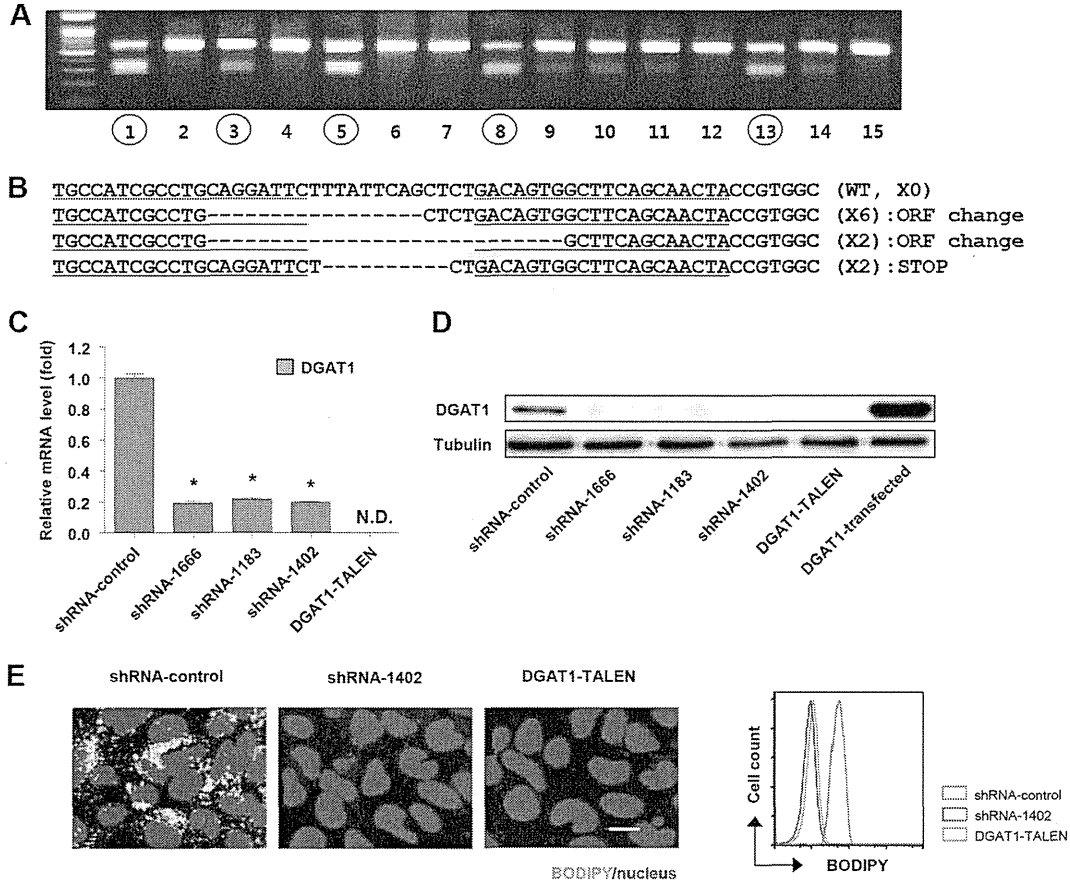

FIG 1 Establishment of DGAT1-silenced cell lines using DGAT1-TALEN or lentivirus vector shRNA DGAT1. (A) Huh-7.5 cells were transfected with plasmids encoding a pair of *DGAT1*-targeting TALENs in combination with the reporter encoding H-2K^k. After the magnetic sorting of cells with TALEN-driven mutations, we analyzed 62 single-cell-derived colonies using the T7E1 assay. The region of the DGAT1 gene containing the TALEN target site was amplified by nested PCR and visualized by agarose gel electrophoresis. Representative data from the T7E1 assay are presented here. Circled numbers indicate clones that were selected for *DGAT1* gene sequencing. (B) DNA sequences of the DGAT1-TALEN cell line. The sequence presented here is part of the *DGAT1* gene of clone 13, one of the clones that are presented in panel A. Zinc finger nuclease recognition sites are underlined, and deleted bases are indicated by dashes. TGA, the premature stop codon, is shaded in gray. Clone 13 has a shifted open reading frame (ORF) or premature stop codon in the *DGAT1* gene. (C) DGAT1 mRNA levels were determined by real-time quantitative PCR in DGAT1-silenced cell lines and standardized to β-actin mRNA levels (n = 3). N.D., not detected. (D) DGAT1 protein expression in DGAT1-silenced cell lines was assessed by immunoblotting. (E) Intracellular lipid droplet staining was performed using the BODIPY lipid probe 493/503 in the control and DGAT1-silenced cell lines. The scale bar represents 20 μm. The right panel represents flow cytometry analyses of the same cell lines.

cells (Fig. 2A). We also quantified intracellular HCV RNA copies and unexpectedly discovered that the intracellular HCV RNA titer was very low in the DGAT1-silenced cell lines (Fig. 2B). Following inoculation of the DGAT1-silenced cell lines with a higher dose of JFH-1, we detected no intracellular HCV core protein by flow cytometry (Fig. 2C).

Next, we transfected the control and DGAT1-silenced cell lines with JFH-1 RNA. As expected from the previous study (11) and loss of intracellular lipid droplets in the DGAT1-silenced cell lines, the production of infectious virions was severely impaired in the DGAT1-silenced cell lines (Fig. 2D). The intracellular HCV RNA copy number was also lower in the DGAT1-silenced cell lines than in the control cell line, with a difference of less than 1 log (Fig. 2E), indicating that HCV RNA replication is slightly impaired in DGAT1-silenced cells. However, this minor decrease is in contrast to the enormous decrease that was observed in the HCVcc inoculation study (Fig. 2B). This finding indicates that another factor is the major cause of the very low intracellular HCV RNA levels in HCVcc-inoculated, DGAT1-silenced cells.

With the hypothesis that HCV entry is defective in DGAT1-silenced cell lines, we evaluated HCV entry using HCVpp of various genotypes. No HCVpp entered the DGAT1-silenced cell lines (Fig. 2F), whereas the control virus pseudoparticles with VSV-G did enter these lines, indicating that HCV entry is impaired in the absence of DGAT1.

Claudin-1 expression is downregulated in DGAT1-silenced cell lines. Because of the impaired HCV entry into DGAT1-silenced cell lines, we investigated the expression of host proteins participating in HCV entry, including tetraspanin CD81 (28), the high-density lipoprotein receptor scavenger receptor class B type I (SR-BI) (29), and two tight junction proteins, claudin-1 (CLDN1) (30) and occludin (OCLN) (31). In the flow cytometric analysis, the expression of CD81, SR-BI, and OCLN in DGAT1-silenced cell lines was well preserved, but that of CLDN1 was markedly diminished (Fig. 3A and B). We observed the downregulation of CLDN1 expression at the mRNA level by real-time quantitative PCR (Fig. 3C). Immunoblotting confirmed the downregulation of CLDN1 expression (Fig. 3D). Notably, CLDN1 expression was

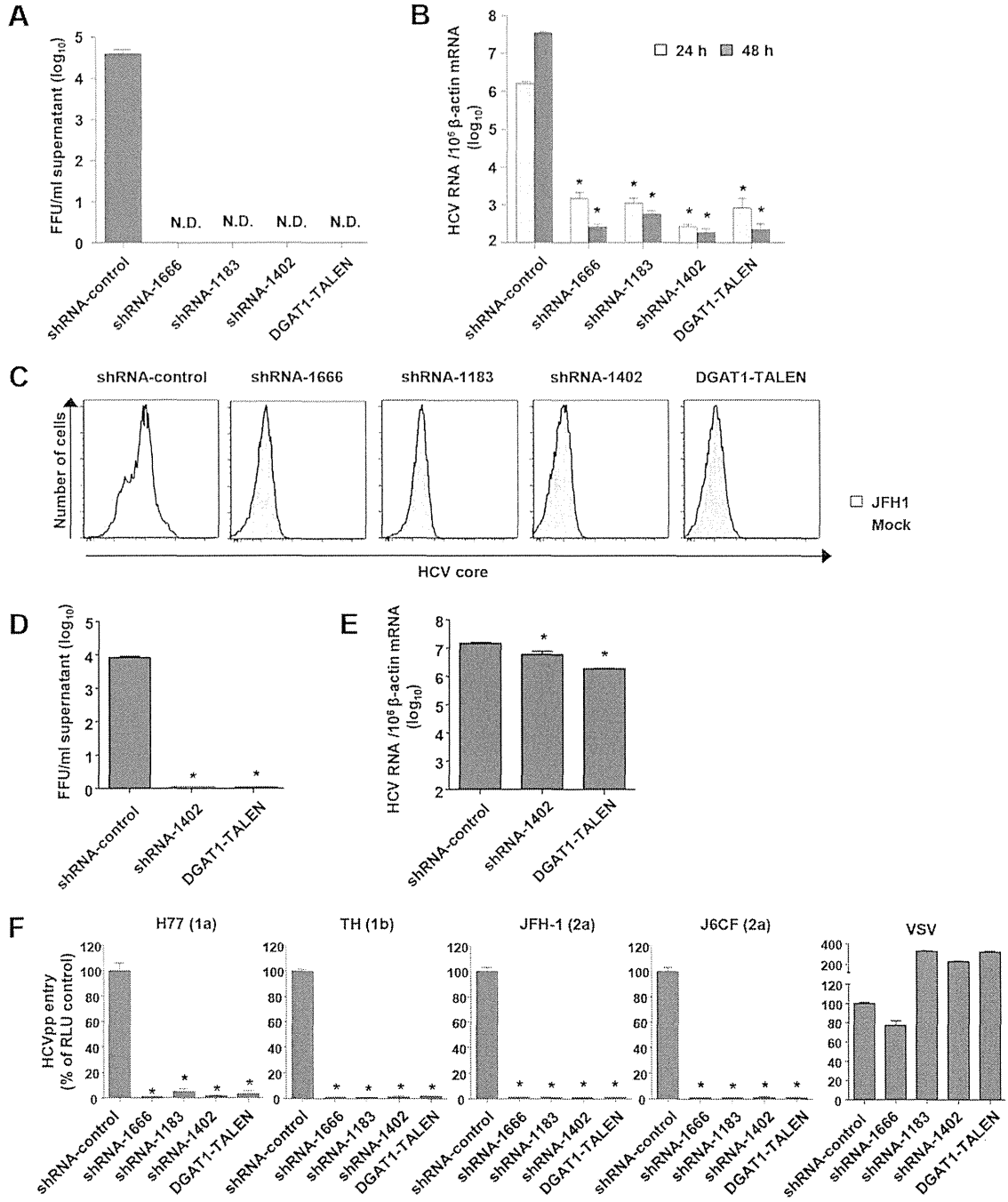

FIG 2 HCV entry into DGAT1-silenced Huh-7.5 cell lines is impaired. (A and B) DGAT1-silenced cell lines were inoculated with JFH-1 HCVcc at a multiplicity of infection (MOI) of 0.1. After 72 h, infectious HCV virions were quantified in culture supernatants by a colorimetric focus-forming assay (19). The data are presented as focus-forming units (FFU) per ml of culture supernatant ($n = 3$) (A). Intracellular HCV RNA levels were determined by real-time quantitative PCR and standardized to β-actin mRNA levels ($n = 3$) (B). (C) DGAT1-silenced cell lines were inoculated with JFH-1 HCVcc at an MOI of 0.5. After 60 h, intracellular HCV core proteins were detected by flow cytometry. Data are representative of two independent experiments. (D and E) DGAT1-silenced cell lines were transfected with 5 μg *in vitro*-transcribed JFH1 RNA. After 72 h, infectious HCV virions were quantified in culture supernatants by a colorimetric focus-forming assay (19). The data are presented as focus-forming units (FFU) per ml of culture supernatant ($n = 3$) (D). Intracellular HCV RNA levels were determined by real-time quantitative PCR and standardized to β-actin mRNA levels ($n = 3$) (E). (F) HCV entry into DGAT1-silenced cell lines was assessed using HCVpp harboring E1 and E2 glycoproteins of various HCV genotypes. Virus pseudoparticles harboring the vesicular stomatitis virus G (VSV-G) envelope glycoprotein were used as a positive control. HCVpp entry was determined by luciferase activity. Data are expressed as percentages of the shRNA-control cell line ($n = 3$). Bar graphs represent means ± SEM. *, $P < 0.001$ compared to the control. N.D., not detected.

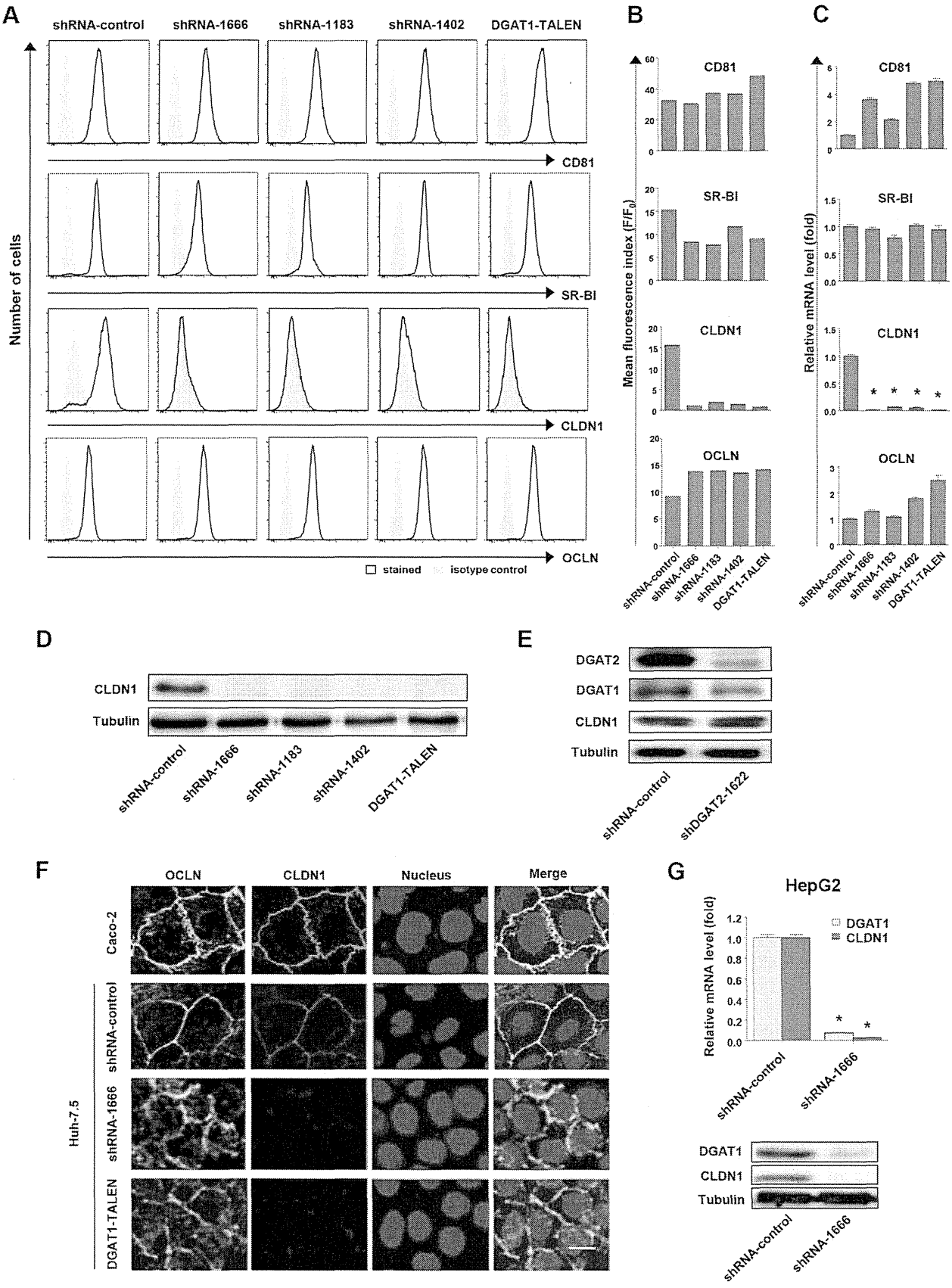

FIG 3 CLDN1 expression is downregulated in DGAT1-silenced cell lines. (A and B) The expression of CD81, SR-B1, CLDN1, and OCLN in DGAT1-silenced cell lines was analyzed by flow cytometry. Histograms are representative of three independent experiments (A), and the mean fluorescence index (F/F_0) of the

not downregulated by the silencing of DGAT2, the other DGAT protein present in human hepatocytes (Fig. 3E). Immunofluorescence staining revealed that CLDN1 expression on the cell membrane was lost in the DGAT1-silenced cells (Fig. 3F). Additionally, a significant proportion of OCLN was localized not only to the cell membrane but also to the cytoplasm in these cells (Fig. 3F). We further confirmed downregulation of CLDN1 at the mRNA and protein levels under DGAT1-silencing conditions in another hepatoma cell line, HepG2, following DGAT1 silencing by lentivirus shRNA transduction (Fig. 3G).

Forced expression of CLDN1 restores HCV entry to DGAT1-silenced cell lines. To verify whether the downregulation of CLDN1 expression led to HCV entry impairment, we transfected DGAT1-silenced cell lines with the *CLDN1* gene and evaluated HCV entry using HCVpp. After 72 h of the transfection, CLDN1 expression was observed by immunoblotting (Fig. 4A) and flow cytometry (Fig. 4B). Importantly, the entry of all of the HCVpp was restored in the CLDN1-expressing DGAT1-silenced cells (Fig. 4C). These results demonstrate that CLDN1 downregulation is responsible for impairment of HCV entry into DGAT1-silenced cells and that the reexpression of CLDN1 is sufficient to restore HCV entry into these cells.

Expression of hepatocyte-specific genes is reduced in DGAT1-silenced cell lines. In DGAT1-silenced cells, we examined the expression of hepatocyte nuclear factor 4α (HNF4α) because this factor has been reported to be associated with CLDN1 expression in mice (32–34). In fact, HNF4α expression was markedly reduced in DGAT1-silenced cell lines at both the mRNA and protein levels (Fig. 5A). HNF4α is a central regulator of hepatocyte differentiation and function (35, 36), and the expression of other hepatocyte-specific genes, such as the albumin and α1-antitrypsin genes, was also decreased in the DGAT1-silenced cells (Fig. 5B), suggesting that their differentiation status had been altered by DGAT1 silencing. However, HNF4α expression was not downregulated by the silencing of DGAT2 (Fig. 5C). We also examined temporal changes in DGAT1, HNF4α, and CLDN1 expression during the establishment of a stable cell line following lentivirus shRNA-DGAT1 transduction into Huh-7.5 cells. DGAT1 expression was silenced at 10 days following transduction, whereas the expression of HNF4α and CLDN1 was preserved (Fig. 5D). HNF4α expression then decreased gradually, followed by a slow decrease in CLDN1 expression. Ultimately, the expression of both HNF4α and CLDN1 was markedly diminished at 45 days following transduction (Fig. 5D).

To verify whether DGAT1 silencing directly caused the downregulation of HNF4α and CLDN1, we transfected shRNA-DGAT1-transduced cells with the shRNA-resistant *DGAT1* gene 10 days after the transduction. Following the transfection, DGAT1 expression was restored, and expression of HNF4α and CLDN1 was maintained (Fig. 6A). In addition, intracellular lipid droplets were restored by transfection (Fig. 6B). Furthermore, HCVpp entry was recovered by the restoration of DGAT1 expression (Fig. 6C). Next, we examined the requirement for the catalytic activity of DGAT1 for the maintenance of CLDN1 and HNF4α expression. We constructed a catalytically inactive *DGAT1* mutant gene (H415A) (11, 37) that was also shRNA resistant. Unlike the catalytically active DGAT1, the catalytically inactive form did not maintain the expression of CLDN1 and HNF4α (Fig. 6D). Collectively, these results indicate that DGAT1 silencing causes HNF4α and CLDN1 downregulation and HCV entry impairment and that the loss of DGAT1 catalytic activity is important in this process.

As HNF4α was reported to upregulate CLDN1 expression in mice (32, 33), we examined whether HNF4α downregulation was responsible for the CLDN1 downregulation that was observed in the DGAT1-silenced cells. In fact, HNF4α bound to the promoter region of human *CLDN1* in the ChIP assay (Fig. 6E and F). However, HNF4α silencing by siRNA (siHNF4α) did not significantly decrease CLDN1 expression (Fig. 6G and H). We also transfected DGAT1-silenced cells with the *HNF4α* gene. For the transfection, we used the gene encoding HNF4α1, which is a major isoform in adult human hepatocytes (38, 39). However, CLDN1 expression was not restored by this transfection (Fig. 6I). Taking these findings together, we conclude that CLDN1 expression is not regulated solely by HNF4α but also by other factors that are influenced by DGAT1 silencing.

Exogenous palmitic acid treatment prevents downregulation of CLDN1 and HNF4α expression after DGAT1 silencing. Considering that DGAT1 regulates intracellular lipid homeostasis (10) and our data showing that intracellular lipid droplets are depleted in DGAT1-silenced cells (Fig. 1E), we hypothesized that CLDN1 downregulation might be attributed to a dysregulation of intracellular fatty acid metabolism. Therefore, we examined the effect of exogenous fatty acid treatment following DGAT1 silencing. We applied BSA-conjugated palmitic acid ($C_{16:0}$) at a low concentration to shRNA-DGAT1-transduced cells 10 days after the transduction and continued the treatment for 17 days. The expression of CLDN1 and HNF4α was preserved by palmitic acid treatment, although DGAT1 expression was silenced (Fig. 7A). Importantly, HCVpp entry was also recovered by palmitic acid treatment (Fig. 7B). These results indicate that altered fatty acid homeostasis in DGAT1-silenced cells is associated with CLDN1 downregulation, which leads to HCV entry impairment.

DISCUSSION

In the present study, we attempted to identify the effects of complete, long-term silencing of DGAT1 on the whole life cycle of HCV in Huh-7.5 cells. We demonstrated that CLDN1 downregulation impairs HCV entry into DGAT1-silenced cell lines and that

histogram is presented (B). F, mean fluorescence intensity (MFI) of specific antibody staining; F_0, MFI of isotype control antibody staining. Data are representative of three independent experiments. (C) mRNA levels of CD81, SR-B1, CLDN1, and OCLN in DGAT1-silenced cell lines were determined by real-time quantitative PCR and standardized to β-actin mRNA levels ($n = 3$). (D) CLDN1 protein expression in DGAT1-silenced cell lines was assessed by immunoblotting. (E) Immunoblot analysis was performed to evaluate CLDN1 expression in the control and DGAT2 knockdown Huh-7.5 cell line after 40 days of shRNA lentiviral transduction. Data are representative of two independent experiments. (F) Immunofluorescence staining was performed using anti-OCLN (green) and anti-CLDN1 (red) in Caco-2, shRNA-control, and DGAT1-silenced Huh-7.5 cell lines, and images were analyzed by confocal microscopy. Merged images are also presented. The scale bar represents 20 μm. (G) A stably DGAT1-silenced HepG2 cell line was established by transduction with a lentivirus harboring shRNA-DGAT1-1666. The mRNA levels of DGAT1 and CLDN1 were determined by real-time quantitative PCR ($n = 3$) (left graph), and the protein expression levels of DGAT1 and CLDN1 were assessed by immunoblotting (right blots). Bar graphs represent means ± SEM. * and **, $P < 0.001$ and $P < 0.01$, respectively, compared to the control.

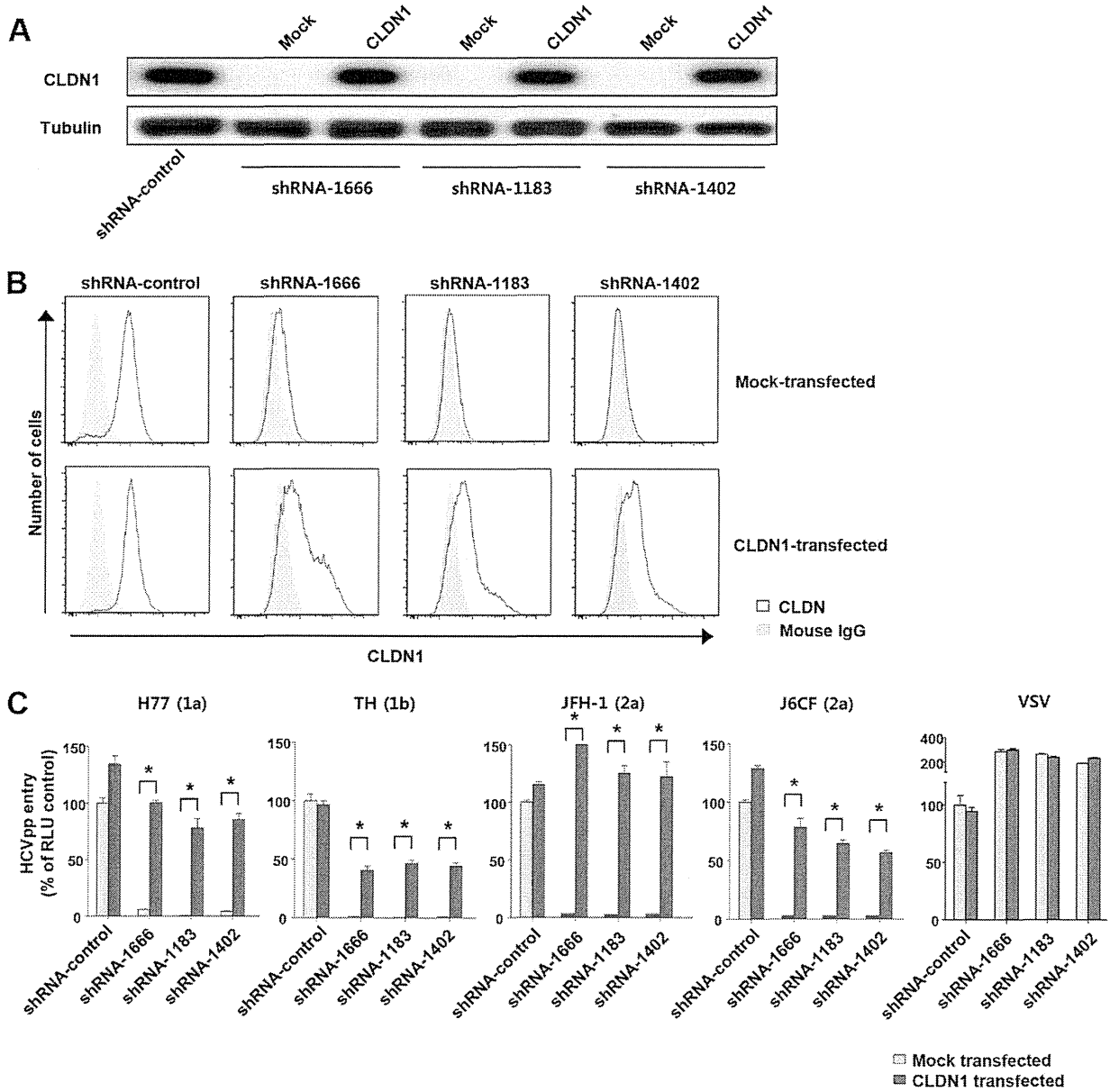

FIG 4 Forced expression of CLDN1 restores HCV entry to DGAT1-silenced cell lines. (A) CLDN1 protein expression was assessed by immunoblotting after mock or CLDN1 transfection of DGAT1-silenced cell lines. (B) Surface expression of CLDN1 was analyzed by flow cytometry after mock or CLDN1 transfection of DGAT1-silenced cell lines. Data are representative of three independent experiments. (C) HCV entry was assessed after mock or CLDN1 transfection of DGAT1-silenced cell lines using HCVpp of various genotypes. Virus pseudoparticles harboring the VSV-G envelope glycoprotein served as a positive control. HCVpp entry was determined by luciferase activity. Data are expressed as percentages of the shRNA-control cell line ($n = 4$). The statistical analysis was conducted for differences between the mock-transfected and CLDN1-transfected cells. Bar graphs represent means ± SEM. *, $P < 0.001$.

this effect is associated with altered fatty acid homeostasis. However, these findings were made using the Huh-7.5 human hepatoma cell line and need to be confirmed in primary human hepatocytes.

One of the main roles of DGAT1 is in catalyzing the final step of triglyceride biosynthesis (5, 6). However, studies of knockout mice have shown that DGAT1 deficiency does not result in elevated levels of diacylglycerol or acyl coenzyme A (acyl-CoA) in the liver, heart, muscle, and adipose tissue following the ingestion of high-fat diets (7, 40). These data suggest that DGAT1 does not simply catalyze the final step of triglyceride biosynthesis but is involved in the regulation of intracellular lipid homeostasis. In fact, DGAT1 recycles the products of triglyceride hydrolysis, which are partial glycerides, for triglyceride synthesis. In addition, DGAT1 inhibition decreases the intracellular lipid pool comprised of triglycerides, partial glycerides, and free fatty acids in human liver-derived cells (10, 41). In the present study, a low-dose exogenous palmitic acid treatment prevented the down-regulation of CLDN1 and HNF4α expression in DGAT1-silenced cells. These results show that expression of CLDN1 and HNF4α is regulated by altered intracellular lipid homeostasis in DGAT1-silenced cells and that the restoration of intracellular fatty acid levels by exogenous palmitic acid rescued CLDN1 and HNF4α expression.

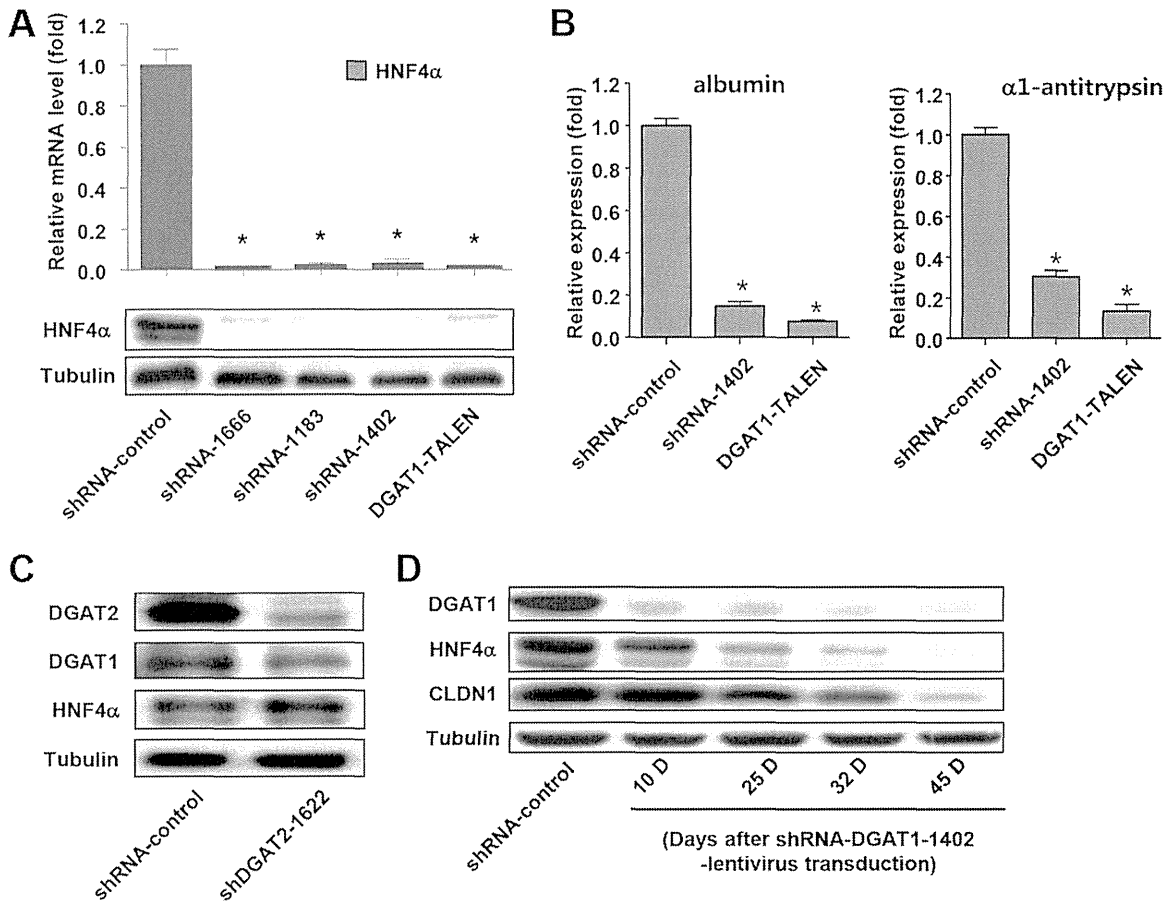

FIG 5 Expression of hepatocyte-specific genes is reduced in DGAT1-silenced cell lines. (A) HNF4α mRNA levels in DGAT1-silenced cell lines were determined by real-time quantitative PCR ($n = 3$) (upper graph), and HNF4α protein expression was assessed by immunoblotting (lower blots). (B) mRNA expression of representative hepatic differentiation markers in control and DGAT1-silenced cell lines. Data are standardized to β-actin mRNA levels ($n = 3$). Bar graphs represent means ± SEM. *, $P < 0.001$ compared to the control. (C) Immunoblot analysis was performed to evaluate HNF4α expression in control and DGAT2 knockdown Huh-7.5 cell lines after 40 days of lentivirus shRNA transduction. Data are representative of two independent experiments. (D) Huh-7.5 cells were transduced with lentivirus harboring shRNA-DGAT1-1402, and temporal changes in protein expression were examined during the establishment of a stable cell line. The cell pellets were harvested at days 10, 25, 32, and 45 after transduction and subjected to immunoblot analyses to detect DGAT1, HNF4α, and CLDN1. Data are representative of two independent experiments.

We also made a DGAT2-silenced cell line in this study. However, the expression of CLDN1 and HNF4α was not downregulated in the DGAT2-silenced cells (Fig. 3E and 5C). DGAT2 also catalyzes the final step of triglyceride synthesis, but recent reports suggest that DGAT1 and DGAT2 play different roles in human hepatocytes (10). DGAT2 is involved in the *de novo* synthesis of triglycerides, whereas DGAT1 functions in the reesterification of partial glycerides that are generated by intracellular lipolysis. Moreover, DGAT2 encompasses 30% of the total DGAT activity in human hepatocytes, whereas DGAT1 contributes the other 70% (10).

HNF4α is a central regulator of hepatocyte differentiation and function (33, 34) and is a major transcription factor that regulates the expression of genes that are involved in lipid homeostasis (42). HNF4α is also known to regulate the expression of proteins that are required for hepatic and intestinal tight junction assembly, including CLDN1, in mice (30–32). A recent study demonstrated the binding of HNF4α to the CLDN1 gene by an electrophoretic mobility shift assay and ChIP assay of the mouse fetal liver (30). In accordance with this previous report, our present data showed that HNF4α bound to the promoter region of human *CLDN1* in a ChIP assay (Fig. 6E and F). However, HNF4α silencing did not significantly decrease CLDN1 expression (Fig. 6G and H), and *HNF4α1* transfection did not restore CLDN1 expression in DGAT1-silenced cells (Fig. 6I). Taking these findings together, we conclude that CLDN1 expression is not regulated solely by HNF4α but also by other factors that are influenced by DGAT1 silencing.

A previous study has shown that DGAT1 is involved in the assembly of HCV by facilitating the trafficking of the HCV core protein to the lipid droplet (11). The authors suppressed DGAT1 activity by using a DGAT1 inhibitor or silenced DGAT1 expression by shRNA, but they observed no impairment of HCV entry to Huh-7.5 cells. The discrepancy between the studies may be explained by the duration of DGAT1 inhibition or silencing. The earlier study involved the use of the DGAT inhibitor for a short duration of approximately 72 h. In contrast, we used stable DGAT1-silenced cell lines to study the long-term effects of DGAT1 silencing. In fact, CLDN1 expression decreased gradually in shRNA-DGAT1-transduced cells and was markedly downregu-

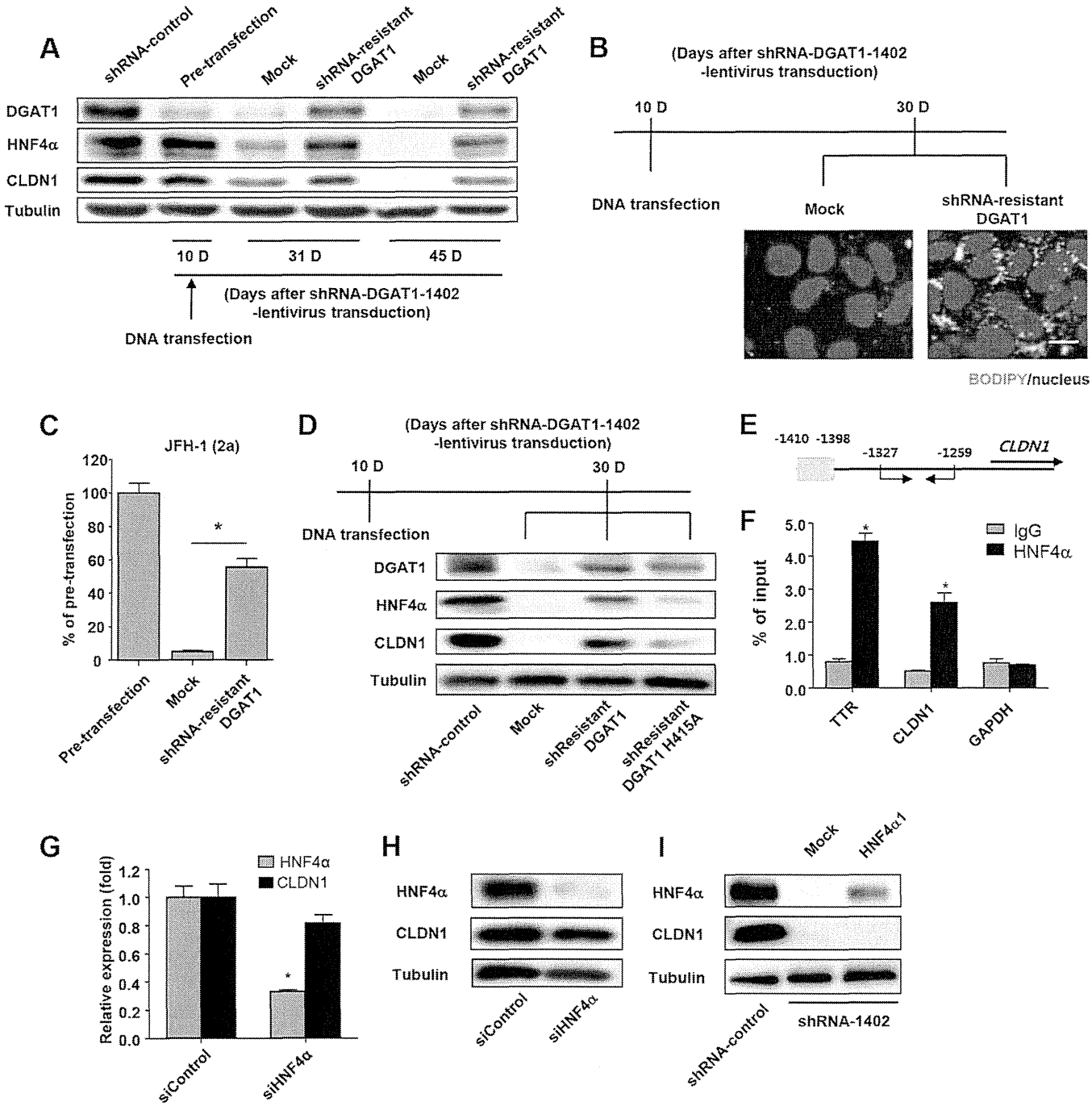

FIG 6 Catalytically active DGAT1 is responsible for maintaining CLDN1 expression and the hepatocyte-specific phenotype in Huh-7.5 cells. (A) An shRNA-1402-resistant *DGAT1* gene was constructed by introducing 6 point mutations into the sequence that is recognized by the shRNA-1402 oligonucleotide without altering the amino acid sequence. The shRNA-1402-resistant *DGAT1* gene was transfected into shRNA-DGAT1-1402-harboring cells 10 days after transduction, and temporal changes in protein expression were examined. The cell pellets were harvested at days 10, 31, and 45 after transduction with lentivirus harboring shRNA-DGAT1-1402 (days 0, 21, and 35 after the shRNA-1402-resistant DGAT1 transfection) and were subjected to immunoblot analysis to detect DGAT1, HNF4α, and CLDN1. Data are representative of two independent experiments. (B) Intracellular lipid droplet staining was performed using the BODIPY lipid probe 493/503 in cells that had been transfected with mock or shRNA-resistant DGAT1. The scale bar represents 20 μm. (C) HCV entry into DGAT1-silenced cell lines was assessed after mock or shRNA-resistant DGAT1 transfection using JFH1 HCVpp. Data are expressed as percentages of the pretransfected cell line ($n = 3$). Bar graphs represent means ± SEM. *, $P < 0.001$. (D) Immunoblot analysis of DGAT1-silenced cell lines harboring a catalytically active or inactive DGAT1 gene was performed. A catalytically inactive DGAT1-encoding plasmid was constructed by site-directed mutagenesis, replacing the histidine residue at position 415 (encoded by CAU) with alanine (encoded by GCU), and the catalytically inactive *DGAT1* gene was also shRNA resistant. We confirmed the sequence of the mutated construct, which was then used to transfect Huh-7.5 cells on 10 days after DGAT1 silencing. Data are representative of two independent experiments. (E, F) The chromatin immunoprecipitation assay was performed using anti-HNF4α antibody. In the schematic of the CLDN1 promoters, the putative HNF4α binding site is shaded in gray, and the positions of the primers for real-time qPCR are designated with arrows (E). Real-time qPCR analysis was performed using DNA precipitated by rabbit anti-HNF4α (clone number H171) (Santa Cruz Biotechnology, Inc.) or IgG. Transthyretin (TTR) was used as a positive control (F). *, $P < 0.01$ ($n = 3$). (G) Real-time qPCR analysis of HNF4α and CLDN1 expression in the Huh-7.5 cell line was conducted after siHNF4α treatment. Data are standardized to β-actin mRNA levels ($n = 3$). Bar graphs represent means ± SEM. *, $P < 0.001$. (H) Immunoblot analysis of HNF4α and CLDN1 in the Huh-7.5 cell line was performed after siHNF4α treatment. Data are representative of two independent experiments. (I) Immunoblot analysis of HNF4α and CLDN1 in DGAT1-silenced cell lines was performed at 72 h after transfection with HNF4α1 plasmid. Data are representative of two independent experiments.

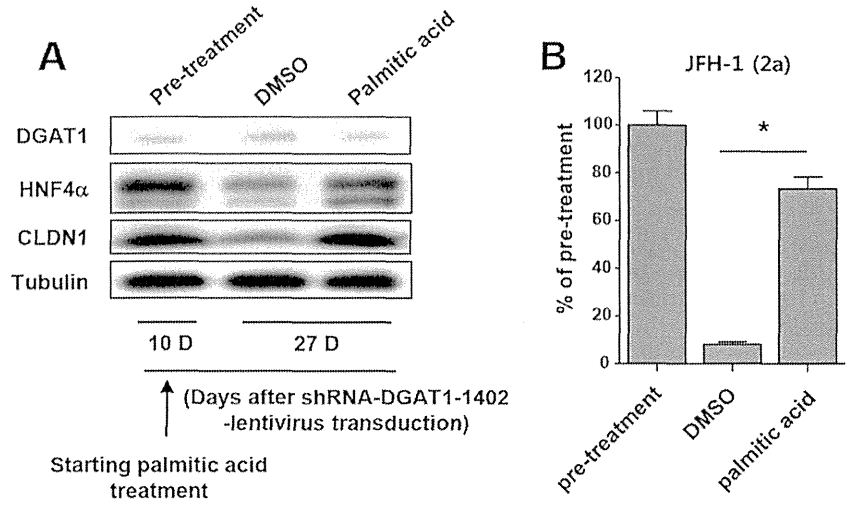

FIG 7 Exogenous palmitic acid treatment prevents downregulation of CLDN1 and HNF4α expression after DGAT1 silencing. (A) From day 10 after transduction with lentiviruses harboring shRNA-DGAT1-1402, the transduced cells were cultured in medium that had been supplemented with 10% charcoal-stripped fetal bovine serum and 1% bovine serum albumin with either 50 μM palmitic acid or DMSO. The cell pellets were harvested at days 10 and 27 after transduction (days 0 and 17 after the palmitic acid treatment) and subjected to immunoblot analysis to detect DGAT1, HNF4α, and CLDN1. Data are representative of two independent experiments. (B) HCV entry (of JFH1 HCVpp) into DGAT1-silenced cell lines was assessed after DMSO or palmitic acid treatment. Data are expressed as percentages of the values for the pretreatment cell lines ($n = 3$). Bar graphs represent means ± SEM. *, $P < 0.001$.

lated only after long-term culturing for over 45 days (Fig. 5D). In the present study, we also knocked out the *DGAT1* gene by using the TALEN technique to silence DGAT1 expression completely and found no DGAT1 expression in the DGAT1-TALEN cell line (Fig. 1C and D). Interestingly, DGAT1-TALEN transfection facilitated CLDN1 downregulation compared to shRNA-DGAT1 transduction in the process of stable cell line establishment (data not shown). CLDN1 downregulation may be induced only by the complete silencing of DGAT1, which could be achieved by a long-term culture of shRNA-DGAT1-transduced cells or by highly efficient silencing with DGAT1-TALEN.

In the present study, we found that HCV RNA replication was also slightly impaired in DGAT1-silenced cell lines (Fig. 2E). This impairment can be partially attributed to the loss of lipid droplets in these cells (Fig. 1E). In fact, recent studies have emphasized the association of lipid droplets and HCV RNA replication (43). Further research is required to clarify the manner by which HCV RNA replication is influenced by intracellular fatty acid homeostasis.

In conclusion, our data demonstrate that complete, long-term silencing of DGAT1 causes CLDN1 downregulation and thus inhibits HCV entry and that CLDN1 downregulation is associated with altered fatty acid homeostasis in the absence of DGAT1. Future research is needed to elucidate the exact mechanisms and consequences of CLDN1 downregulation in DGAT1-silenced hepatocytes.

ACKNOWLEDGMENTS

This work was supported by a National Agenda Project grant from the Korea Research Council of Fundamental Science and Technology (NTM1311423), the Korea Research Institute for Bioscience and Biotechnology (KRIBB) Initiative Program (KGM3121423), and by the Project of Global Ph.D. Fellowship (NRF-2012H1A2A1012809, to P.S.S.) through the National Research Foundation of Korea (NRF) funded by the Ministry of Science, ICT, and Future Planning of Korea. A.M. and T.K. were supported by a grant-in-aid from the Japan Society for the Promotion of Science and from the Ministry of Health, Labor, and Welfare of Japan. This work was partly supported by the KAIST (Korea Advanced Institute of Science and Technology) Future Systems Healthcare Project from the Ministry of Science, ICT, and Future Planning of Korea.

REFERENCES

1. Lavanchy D. 2011. Evolving epidemiology of hepatitis C virus. Clin. Microbiol. Infect. 17:107–115. http://dx.doi.org/10.1111/j.1469-0691.2010.03432.x.
2. Liang TJ, Ghany MG. 2013. Current and future therapies for hepatitis C virus infection. N. Engl. J. Med. 368:1907–1917. http://dx.doi.org/10.1056/NEJMra1213651.
3. Aloia AL, Locarnini S, Beard MR. 2012. Antiviral resistance and direct-acting antiviral agents for HCV. Antivir. Ther. 17:1147–1162. http://dx.doi.org/10.3851/IMP2426.
4. Zeisel MB, Lupberger J, Fofana I, Baumert TF. 2013. Host-targeting agents for prevention and treatment of chronic hepatitis C—perspectives and challenges. J. Hepatol. 58:375–384. http://dx.doi.org/10.1016/j.jhep.2012.09.022.
5. Cases S, Smith SJ, Zheng YW, Myers HM, Lear SR, Sande E, Novak S, Collins C, Welch CB, Lusis AJ, Erickson SK, Farese RV, Jr. 1998. Identification of a gene encoding an acyl CoA:diacylglycerol acyltransferase, a key enzyme in triacylglycerol synthesis. Proc. Natl. Acad. Sci. U. S. A. 95:13018–13023. http://dx.doi.org/10.1073/pnas.95.22.13018.
6. Yen CL, Stone SJ, Koliwad S, Harris C, Farese RV, Jr. 2008. Thematic review series: glycerolipids. DGAT enzymes and triacylglycerol biosynthesis. J. Lipid Res. 49:2283–2301. http://dx.doi.org/10.1194/jlr.R800018-JLR200.
7. Smith SJ, Cases S, Jensen DR, Chen HC, Sande E, Tow B, Sanan DA, Raber J, Eckel RH, Farese RV, Jr. 2000. Obesity resistance and multiple mechanisms of triglyceride synthesis in mice lacking Dgat. Nat. Genet. 25:87–90. http://dx.doi.org/10.1038/75651.
8. Devita RJ, Pinto S. 3 September 2013. Current status of the research and development of diacylglycerol O-acyltransferase 1 (DGAT1) inhibitors. J. Med. Chem. http://dx.doi.org/10.1021/jm4007033.
9. Haas JT, Winter HS, Lim E, Kirby A, Blumenstiel B, DeFelice M, Gabriel S, Jalas C, Branski D, Grueter CA, Toporovski MS, Walther TC, Daly MJ, Farese RV, Jr. 2012. DGAT1 mutation is linked to a congenital diarrheal disorder. J. Clin. Invest. 122:4680–4684. http://dx.doi.org/10.1172/JCI64873.
10. Wurie HR, Buckett L, Zammit VA. 2012. Diacylglycerol acyltransferase 2 acts upstream of diacylglycerol acyltransferase 1 and utilizes nascent diglycerides and de novo synthesized fatty acids in HepG2 cells. FEBS J. 279:3033–3047. http://dx.doi.org/10.1111/j.1742-4658.2012.08684.x.

11. Herker E, Harris C, Hernandez C, Carpentier A, Kaehlcke K, Rosenberg AR, Farese RV, Jr, Ott M. 2010. Efficient hepatitis C virus particle formation requires diacylglycerol acyltransferase-1. Nat. Med. 16:1295–1298. http://dx.doi.org/10.1038/nm.2238.
12. Camus G, Herker E, Modi AA, Haas JT, Ramage HR, Farese RV, Jr, Ott M. 2013. Diacylglycerol acyltransferase-1 localizes hepatitis C virus NS5A protein to lipid droplets and enhances NS5A interaction with the viral capsid core. J. Biol. Chem. 288:9915–9923. http://dx.doi.org/10.1074/jbc.M112.434910.
13. Blight KJ, McKeating JA, Rice CM. 2002. Highly permissive cell lines for subgenomic and genomic hepatitis C virus RNA replication. J. Virol. 76:13001–13014. http://dx.doi.org/10.1128/JVI.76.24.13001-13014.2002.
14. Kato T, Miyamoto M, Furusaka A, Date T, Yasui K, Kato J, Matsushima S, Komatsu T, Wakita T. 2003. Processing of hepatitis C virus core protein is regulated by its C-terminal sequence. J. Med. Virol. 69:357–366. http://dx.doi.org/10.1002/jmv.10297.
15. Lindenbach BD, Evans MJ, Syder AJ, Wölk B, Tellinghuisen TL, Liu CC, Maruyama T, Hynes RO, Burton DR, McKeating JA, Rice CM. 2005. Complete replication of hepatitis C virus in cell culture. Science 309:623–626. http://dx.doi.org/10.1126/science.1114016.
16. Wakita T, Pietschmann T, Kato T, Date T, Miyamoto M, Zhao Z, Murthy K, Habermann A, Kräusslich HG, Mizokami M, Bartenschlager R, Liang TJ. 2005. Production of infectious hepatitis C virus in tissue culture from a cloned viral genome. Nat. Med. 11:791–796. http://dx.doi.org/10.1038/nm1268.
17. Zhong J, Gastaminza P, Cheng G, Kapadia S, Kato T, Burton DR, Wieland SF, Uprichard SL, Wakita T, Chisari FV. 2005. Robust hepatitis C virus infection in vitro. Proc. Natl. Acad. Sci. U. S. A. 102:9294–9299. http://dx.doi.org/10.1073/pnas.0503596102.
18. Park J, Kang W, Ryu SW, Kim WI, Chang DY, Lee DH, Park DY, Choi Y-H, Choi K, Shin E-C, Choi C. 2012. Hepatitis C virus infection enhances TNFalpha-induced cell death via suppression of NF-kappaB. Hepatology 56:831–840. http://dx.doi.org/10.1002/hep.25726.
19. Kang W, Shin EC. 2012. Colorimetric focus-forming assay with automated focus counting by image analysis for quantification of infectious hepatitis C virions. PLoS One 7:e43960. http://dx.doi.org/10.1371/journal.pone.0043960.
20. Bartosch B, Dubuisson J, Cosset FL. 2003. Infectious hepatitis C virus pseudo-particles containing functional E1-E2 envelope protein complexes. J. Exp. Med. 197:633–642. http://dx.doi.org/10.1084/jem.20021756.
21. Matsumura T, Kato T, Sugiyama N, Tasaka-Fujita M, Murayama A, Masaki T, Wakita T, Imawari M. 2012. 25-Hydroxyvitamin D3 suppresses hepatitis C virus production. Hepatology 56:1231–1239. http://dx.doi.org/10.1002/hep.25763.
22. Kim Y, Kweon J, Kim A, Chon JK, Yoo JY, Kim HJ, Kim S, Lee C, Jeong E, Chung E, Kim D, Lee MS, Go EM, Song HJ, Kim H, Cho N, Bang D, Kim S, Kim JS. 2013. A library of TAL effector nucleases spanning the human genome. Nat. Biotechnol. 31:251–258. http://dx.doi.org/10.1038/nbt.2517.
23. Kim H, Kim MS, Wee G, Lee CI, Kim H, Kim JS. 2013. Magnetic separation and antibiotics selection enable enrichment of cells with ZFN/TALEN-induced mutations. PLoS One 8:e56476. http://dx.doi.org/10.1371/journal.pone.0056476.
24. Doyon Y, Choi VM, Xia DF, Vo TD, Gregory PD, Holmes MC. 2010. Transient cold shock enhances zinc-finger nuclease-mediated gene disruption. Nat. Methods 7:459–460. http://dx.doi.org/10.1038/nmeth.1456.
25. Takeuchi T, Katsume A, Tanaka T, Abe A, Inoue K, Tsukiyama-Kohara K, Kawaguchi R, Tanaka S, Kohara M. 1999. Real-time detection system for quantification of hepatitis C virus genome. Gastroenterology 116:636–642. http://dx.doi.org/10.1016/S0016-5085(99)70185-X.
26. Fang B, Mane-Padros D, Bolotin E, Jiang T, Sladek FM. 2012. Identification of a binding motif specific to HNF4 by comparative analysis of multiple nuclear receptors. Nucleic Acids Res. 40:5343–5356. http://dx.doi.org/10.1093/nar/gks190.
27. Runkle EA, Rice SJ, Qi J, Masser D, Antonetti DA, Winslow MM, Mu D. 2012. Occludin is a direct target of thyroid transcription factor-1 (TTF-1/NKX2–1). J. Biol. Chem. 287:28790–287801. http://dx.doi.org/10.1074/jbc.M112.367987.
28. Pileri P, Uematsu Y, Campagnoli S, Galli G, Falugi F, Petracca R, Weiner AJ, Houghton M, Rosa D, Grandi G, Abrignani S. 1998. Binding of hepatitis C virus to CD81. Science 282:938–941. http://dx.doi.org/10.1126/science.282.5390.938.
29. Scarselli E, Ansuini H, Cerino R, Roccasecca RM, Acali S, Filocamo G, Traboni C, Nicosia A, Cortese R, Vitelli A. 2002. The human scavenger receptor class B type I is a novel candidate receptor for the hepatitis C virus. EMBO J. 21:5017–5025. http://dx.doi.org/10.1093/emboj/cdf529.
30. Evans MJ, von Hahn T, Tscherne DM, Syder AJ, Panis M, Wölk B, Hatziioannou T, McKeating JA, Bieniasz PD, Rice CM. 2007. Claudin-1 is a hepatitis C virus co-receptor required for a late step in entry. Nature 446:801–805. http://dx.doi.org/10.1038/nature05654.
31. Ploss A, Evans MJ, Gaysinskaya VA, Panis M, You H, de Jong YP, Rice CM. 2009. Human occludin is a hepatitis C virus entry factor required for infection of mouse cells. Nature 457:882–886. http://dx.doi.org/10.1038/nature07684.
32. Battle MA, Konopka G, Parviz F, Gaggl AL, Yang C, Sladek FM, Duncan SA. 2006. Hepatocyte nuclear factor 4alpha orchestrates expression of cell adhesion proteins during the epithelial transformation of the developing liver. Proc. Natl. Acad. Sci. U. S. A. 103:8419–8424. http://dx.doi.org/10.1073/pnas.0600246103.
33. Walesky C, Gunewardena S, Terwilliger EF, Edwards G, Borude P, Apte U. 2013. Hepatocyte-specific deletion of hepatocyte nuclear factor-4α in adult mice results in increased hepatocyte proliferation. Am. J. Physiol. Gastrointest. Liver Physiol. 304:G26–G37. http://dx.doi.org/10.1152/ajpgi.00064.2012.
34. Zhong W, Zhao Y, McClain CJ, Kang YJ, Zhou Z. 2010. Inactivation of hepatocyte nuclear factor-4α mediates alcohol-induced downregulation of intestinal tight junction proteins. Am. J. Physiol. Gastrointest. Liver Physiol. 299:G643–G651. http://dx.doi.org/10.1152/ajpgi.00515.2009.
35. Bolotin E, Liao H, Ta TC, Yang C, Hwang-Verslues W, Evans JR, Jiang T, Sladek FM. 2010. Integrated approach for the identification of human hepatocyte nuclear factor 4alpha target genes using protein binding microarrays. Hepatology 51:642–653. http://dx.doi.org/10.1002/hep.23357.
36. Tirona RG, Lee W, Leake BF, Lan LB, Cline CB, Lamba V, Parviz F, Duncan SA, Inoue Y, Gonzalez FJ, Schuetz EG, Kim RB. 2003. The orphan nuclear receptor HNF4alpha determines PXR- and CAR-mediated xenobiotic induction of CYP3A4. Nat. Med. 9:220–224. http://dx.doi.org/10.1038/nm815.
37. Hofmann K. 2000. A superfamily of membrane-bound O-acyltransferases with implications for wnt signaling. Trends Biochem. Sci. 25:111–112. http://dx.doi.org/10.1016/S0968-0004(99)01539-X.
38. Nakhei H, Lingott A, Lemm I, Ryffel GU. 1998. An alternative splice variant of the tissue specific transcription factor HNF4alpha predominates in undifferentiated murine cell types. Nucleic Acids Res. 26:497–504. http://dx.doi.org/10.1093/nar/26.2.497.
39. Babeu JP, Boudreau F. 2014. Hepatocyte nuclear factor 4-alpha involvement in liver and intestinal inflammatory networks. World J. Gastroenterol. 20:22–30. http://dx.doi.org/10.3748/wjg.v20.i1.22.
40. Liu L, Yu S, Khan RS, Ables GP, Bharadwaj KG, Hu Y, Huggins LA, Eriksson JW, Buckett LK, Turnbull AV, Ginsberg HN, Blaner WS, Huang LS, Goldberg IJ. 2011. DGAT1 deficiency decreases PPAR expression and does not lead to lipotoxicity in cardiac and skeletal muscle. J. Lipid Res. 52:732–744. http://dx.doi.org/10.1194/jlr.M011395.
41. Wurie HR, Buckett L, Zammit VA. 2011. Evidence that diacylglycerol acyltransferase 1 (DGAT1) has dual membrane topology in the endoplasmic reticulum of HepG2 cells. J. Biol. Chem. 286:36238–36247. http://dx.doi.org/10.1074/jbc.M111.251900.
42. Hayhurst GP, Lee YH, Lambert G, Ward JM, Gonzalez FJ. 2001. Hepatocyte nuclear factor 4alpha (nuclear receptor 2A1) is essential for maintenance of hepatic gene expression and lipid homeostasis. Mol. Cell. Biol. 21:1393–1403. http://dx.doi.org/10.1128/MCB.21.4.1393-1403.2001.
43. Tanaka T, Kuroda K, Ikeda M, Wakita T, Kato N, Makishima M. 2013. Hepatitis C virus NS4B targets lipid droplets through hydrophobic residues in the amphipathic helices. J. Lipid Res. 54:881–892. http://dx.doi.org/10.1194/jlr.M026443.

Supplementary Figure 1

Silenced genes	Cell line	Oligonucleotide sequence
DGAT1	shRNA-1666	CCGGCGACTACTACGTGCTCAACTACTCGAGTAGTTGAGCACGTAGTAGTCGTTTTTG
	shRNA-1183	CCGGCATGGACTACTCACGCATCATCTCGAGATGATGCGTGAGTAGTCCATGTTTTTG
	shRNA-1402	CCGGCAGACACTTCTACAAGCCCATCTCGAGATGGGCTTGTAGAAGTGTCTGTTTTTG
DGAT2	shRNA-1622	CCGGGTTCTAGGTGGTGGCTAAATCCTCGAGGATTTAGCCACCACCTAGAACTTTTTTG

Sequences of three different shRNA-DGAT1 and shRNA-DGAT2 oligonucleotides.

Underlined parts are the sequences recognized by respective mRNAs.

JVI
Journals.ASM.org

Involvement of Hepatitis C Virus NS5A Hyperphosphorylation Mediated by Casein Kinase I-α in Infectious Virus Production

Takahiro Masaki,[a,e] Satoko Matsunaga,[b] Hirotaka Takahashi,[b] Kenji Nakashima,[d] Yayoi Kimura,[c] Masahiko Ito,[d] Mami Matsuda,[a] Asako Murayama,[a] Takanobu Kato,[a] Hisashi Hirano,[c] Yaeta Endo,[b] Stanley M. Lemon,[e,f,g] Takaji Wakita,[a] Tatsuya Sawasaki,[b] Tetsuro Suzuki[d]

Department of Virology II, National Institute of Infectious Diseases, Toyama, Shinjuku-ku, Tokyo, Japan[a]; Proteo-Science Center, Ehime University, Matsuyama, Ehime, Japan[b]; Graduate School of Medical Life Science and Advanced Medical Research Center, Yokohama City University, Fukuura, Kanazawa-ku, Yokohama, Japan[c]; Department of Infectious Diseases, Hamamatsu University School of Medicine, Handayama, Higashi-ku, Hamamatsu, Japan[d]; Lineberger Comprehensive Cancer Center,[e] Division of Infectious Diseases, Department of Medicine,[f] and Department of Microbiology and Immunology,[g] The University of North Carolina at Chapel Hill, Chapel Hill, North Carolina, USA

ABSTRACT

Nonstructural protein 5A (NS5A) of hepatitis C virus (HCV) possesses multiple functions in the viral life cycle. NS5A is a phosphoprotein that exists in hyperphosphorylated and basally phosphorylated forms. Although the phosphorylation status of NS5A is considered to have a significant impact on its function, the mechanistic details regulating NS5A phosphorylation, as well as its exact roles in the HCV life cycle, are still poorly understood. In this study, we screened 404 human protein kinases via *in vitro* binding and phosphorylation assays, followed by RNA interference-mediated gene silencing in an HCV cell culture system. Casein kinase I-α (CKI-α) was identified as an NS5A-associated kinase involved in NS5A hyperphosphorylation and infectious virus production. Subcellular fractionation and immunofluorescence confocal microscopy analyses showed that CKI-α-mediated hyperphosphorylation of NS5A contributes to the recruitment of NS5A to low-density membrane structures around lipid droplets (LDs) and facilitates its interaction with core protein and the viral assembly. Phospho-proteomic analysis of NS5A with or without CKI-α depletion identified peptide fragments that corresponded to the region located within the low-complexity sequence I, which is important for CKI-α-mediated NS5A hyperphosphorylation. This region contains eight serine residues that are highly conserved among HCV isolates, and subsequent mutagenesis analysis demonstrated that serine residues at amino acids 225 and 232 in NS5A (genotype 2a) may be involved in NS5A hyperphosphorylation and hyperphosphorylation-dependent regulation of virion production. These findings provide insight concerning the functional role of NS5A phosphorylation as a regulatory switch that modulates its multiple functions in the HCV life cycle.

IMPORTANCE

Mechanisms regulating NS5A phosphorylation and its exact function in the HCV life cycle have not been clearly defined. By using a high-throughput screening system targeting host protein kinases, we identified CKI-α as an NS5A-associated kinase involved in NS5A hyperphosphorylation and the production of infectious virus. Our results suggest that the impact of CKI-α in the HCV life cycle is more profound on virion assembly than viral replication via mediation of NS5A hyperphosphorylation. CKI-α-dependent hyperphosphorylation of NS5A plays a role in recruiting NS5A to low-density membrane structures around LDs and facilitating its interaction with the core for new virus particle formation. By using proteomic approach, we identified the region within the low-complexity sequence I of NS5A that is involved in NS5A hyperphosphorylation and hyperphosphorylation-dependent regulation of infectious virus production. These findings will provide novel mechanistic insights into the roles of NS5A-associated kinases and NS5A phosphorylation in the HCV life cycle.

Hepatitis C virus (HCV) is a major causative agent of liver-related morbidity and mortality worldwide and represents a global public health problem (1). An estimated 130 million individuals are chronically infected with HCV worldwide, and the treatment of HCV infection imposes a large economic and societal burden (2). HCV is an enveloped virus with a positive-sense, single-stranded RNA genome in the *Hepacivirus* genus within the *Flaviviridae* family (3). The approximately 9.6-kb genome is translated into a single polypeptide of approximately 3,000 amino acids (aa), which is cleaved by cellular and viral proteases to produce the structural proteins (core, E1, E2, and p7) and nonstructural (NS) proteins (NS2, NS3, NS4A, NS4B, NS5A, and NS5B) (4). NS3 to NS5B are sufficient for RNA replication in cell culture (5). NS5B is an RNA-dependent RNA polymerase (RdRp), and NS3 functions as both an RNA helicase and a serine protease (4). NS4A is the cofactor of the NS3 protease, and the NS3-NS4A complex is required for viral precursor processing (4). NS4B induces the formation of a specialized membrane compartment, a sort of membranous web where viral RNA replication may take

Received 30 October 2013 Accepted 14 April 2014
Published ahead of print 23 April 2014
Editor: M. S. Diamond
Address correspondence to Tetsuro Suzuki, tesuzuki@hama-med.ac.jp.
Supplemental material for this article may be found at http://dx.doi.org/10.1128/JVI.03170-13.

doi:10.1128/JVI.03170-13

place (6). NS5A is essential for both viral RNA replication and virion assembly (7–9).

NS5A is an RNA binding protein and exists as a component of the replicase complex (10–13). NS5A is phosphorylated on multiple serine and threonine residues and can be found in hyperphosphorylated (p58) and basally phosphorylated (p56) forms (14–16). Although the distinct mechanisms for generating p56 and p58 forms are still unclear, it has been reported that two regions located around the center and near the C-terminal regions of NS5A are required for basal phosphorylation, while hyperphosphorylation primarily targets serine residues located within low-complexity sequence I (LCS I), which is the linker between domains I and II (15, 17–19). Several phosphorylation sites have been mapped in NS5A by using recombinantly expressed protein and NS5A extracted from cells harboring subgenomic replicons (20–23).

NS5A phosphorylation plays roles in the regulation of viral RNA replication and virion assembly. Some of the cell culture-adaptive mutations in NS4B and NS5A, which reduce NS5A hyperphosphorylation, have been found to confer efficient replication of genotype 1 replicons in Huh-7 cells (17, 18). Similarly, suppression of NS5A hyperphosphorylation through either the use of kinase inhibitors or mutagenesis allows higher RNA replication in non-culture-adapted replicons (18, 24). In contrast, HCV RNA replication is inhibited after treatment of cells carrying adapted replicons with the same kinase inhibitor (24). The C-terminal domain III of NS5A is not essential for viral RNA replication, but it is important for the production of infectious virus. Alanine replacements of the serine cluster in this domain impair NS5A phosphorylation, leading to a decrease in NS5A-core protein interaction, perturbation of the subcellular distribution of NS5A, and disruption of virion production (7–9).

A number of protein kinases have been identified as having the ability to phosphorylate NS5A based on comprehensive screening by using an RNA interference (RNAi) library, recombinantly expressed kinases, and kinase inhibitors (25–28). Among them, casein kinase I-α (CKI-α) and Polo-like kinase 1 (Plk1) have been shown to play roles in viral RNA replication (25, 27). Although silencing of CKI-α inhibits the replication of the genotype 1b subgenomic replicon containing an adaptive mutation (27), its effect on infectious virus production has not been studied to date. Casein kinase II (CKII) has been identified as a positive regulator of virus production via studies with chemical inhibitors and small interfering RNA (siRNA) (9). However, the functional roles of NS5A phosphorylation by its associated kinases in regulation of the viral life cycle are not yet fully understood.

To identify NS5A-associated kinases involved in the HCV life cycle, we developed an *in vitro*, high-throughput screening system for analyzing protein-protein interactions. Using this system followed by *in vitro* phosphorylation assays, we screened human protein kinases on a kinome-wide scale and identified several NS5A-associated kinases. siRNA experiments showed that silencing of CKI-α leads to the most marked inhibition of infectious virus production among the candidate kinases. Here, we report a novel function of CKI-α in the viral life cycle. It is more likely that CKI-α has a more profound impact on virion assembly than on viral replication through hyperphosphorylation of NS5A. Hyperphosphorylated NS5A was predominantly localized in low-density membrane structures around lipid droplets (LDs), in which NS5A interacts with the core for virion assembly, while reduction of NS5A hyperphosphorylation by siRNA targeting CKI-α led to a decrease in NS5A abundance in the low-density membrane structures. The present study provides important insights into the regulatory roles of NS5A-associated kinases and NS5A phosphorylation in the viral life cycle, especially as a molecular switch governing the transition between viral replication and virion assembly.

MATERIALS AND METHODS

Plasmids. Plasmids pJFH1 and pSGR-JFH1/Luc were generated as previously described (29, 30). The JFH-1-based *Gaussia princeps* luciferase (GLuc) reporter construct, which encodes GLuc followed by the foot-and-mouth disease virus (FMDV) 2A protein between p7 and NS2, was generated in a manner similar to the description in a previous report (31). A 1,042-bp double-stranded DNA fragment containing GLuc (32) and FMDV 2A (33) sequences flanked by BsaI and NotI sites at its ends was synthesized and then inserted into the corresponding sites of pJFH1. Related constructs containing serine-to-alanine or serine-to-aspartic acid mutations in NS5A were generated using oligonucleotide-directed mutagenesis techniques. To construct pCAG-CKI-α, the full-length CKI-α-coding sequence was amplified by PCR using cDNAs prepared from Huh-7 cells. The resulting PCR product was then inserted into the multiple-cloning site of pCAGGS (34). pCAG-CKI-α/m6, which contains six silent point mutations that ablate the binding of CKI-α siRNA but maintain the wild-type amino acid sequence of CKI-α, was generated by oligonucleotide-directed mutagenesis of pCAG-CKI-α. All PCR products were confirmed by automated nucleotide sequencing with an ABI Prism 7000 sequence detection system (Life Technologies, Carlsbad, CA).

Cells. The human hepatoma cell line Huh-7, its derivative cell lines Huh7.5.1 (35) (a gift from Francis V. Chisari, The Scripps Research Institute) and Huh7–25 (36), and the human embryonic kidney cell line 293T used to generate HCV pseudoparticles (HCVpp), were maintained in Dulbecco modified Eagle medium (DMEM) supplemented with nonessential amino acids, 100 U of penicillin/ml, 100 μg of streptomycin/ml, and 10% fetal bovine serum (FBS) at 37°C in a 5% CO_2 incubator. SGR-JFH1/LucNeo cells, which harbor a genotype 2a subgenomic replicon carrying a firefly luciferase reporter gene fused to the neomycin phosphotransferase gene of pSGR-JFH1 (37), and LucNeo#2 cells, which harbor a genotype 1b subgenomic replicon carrying a firefly luciferase/neomycin phosphotransferase fusion reporter gene (38, 39) (a gift from Koichi Watashi, National Institute of Infectious Diseases, and Kunitada Shimotohno, National Center for Global Health and Medicine), were cultured in the above medium supplemented with 300 μg/ml G418.

Antibodies. Mouse monoclonal antibody against core protein (2H9) was generated as described previously (30). Anti-NS5A mouse monoclonal antibody (9E10) was a kind gift from Charles M. Rice (The Rockefeller University), and anti-NS5A rabbit polyclonal antibody (TB0705#1) was developed by immunization with the recombinant NS5A protein (8, 40). For detection of cellular proteins, the following antibodies were used: mouse monoclonal antibodies directed against Plk1 (Life Technologies) and glyceraldehyde 3-phosphate dehydrogenase (GAPDH; Millipore, Temecula, CA); rabbit polyclonal antibodies detecting CKI-α (Santa Cruz Biotechnology, Dallas, TX), CKI-ε (Santa Cruz Biotechnology), cyclinc AMP (cAMP)-dependent protein kinase catalytic subunit β (PKACβ; Santa Cruz Biotechnology), phosphatidylinositol 4-kinase IIIα (PI4K-IIIα; Cell Signaling Technology, Danvers, MA), claudin-1 (CLDN1; Life Technologies), calnexin (Enzo Life Sciences, Farmingdale, NY), and GM130 (Sigma-Aldrich, St. Louis, MO); and goat polyclonal antibodies specific for CKII-α′ (Santa Cruz Biotechnology) and apolipoprotein E (ApoE; Millipore). Fluorescence-conjugated secondary antibodies, including Alexa Fluor 488 goat anti-mouse IgG1 and Alexa Fluor 568 goat anti-mouse IgG2a, were purchased from Life Technologies. Horseradish peroxidase (HRP)-conjugated secondary antibodies were from Cell Signaling Technology.

Protein kinase library and cell-free protein synthesis. The construction and identity of the 404 cDNAs encoding human protein kinases used in this study were previously described (41). *In vitro* transcription and cell-free protein synthesis were performed as previously reported (42, 43). Briefly, DNA templates containing a biotin-ligating sequence were amplified by split-primer PCR with kinase cDNAs and corresponding primers and then used for protein synthesis with a fully automated protein synthesizer, a GenDecoder (CellFree Sciences, Ehima, Japan). For synthesis of FLAG-tagged full-length NS5A and domain III proteins derived from the JFH-1 isolate, DNA templates containing a FLAG sequence were generated from the NS5A expression plasmid (8) by split-primer PCR and used with a wheat germ expression kit (CellFree Sciences) according to the manufacturer's instructions.

Amplified luminescent proximity homogeneous assay (AlphaScreen). FLAG-tagged NS5A proteins were mixed with biotinylated kinases in 15 μl of reaction buffer (20 mM Tris-HCl [pH 7.6], 5 mM $MgCl_2$, 1 mM dithiothreitol, and 1 mg/ml bovine serum albumin) in the wells of 384-well OptiPlates (PerkinElmer, Waltham, MA) and incubated at 26°C for 1 h. The mixture was then added to the detection mixture containing 0.1 μl protein A-conjugated acceptor beads (PerkinElmer), 0.1 μl streptavidin-coated donor beads (PerkinElmer), and 5 μg/ml of the anti-FLAG M2 antibody, followed by incubation at 26°C for 1 h. AlphaScreen signals from the mixture were detected using an EnVision device (PerkinElmer) with the AlphaScreen signal detection program.

***In vitro* phosphorylation assay.** To obtain purified kinases used for *in vitro* phosphorylation assays, DNA templates containing a glutathione *S*-transferase (GST)–tobacco etch virus (TEV) sequence were generated by split-primer PCR with kinase cDNAs and corresponding primers and used in a cell-free production system with the wheat germ expression kit as described above. The GST-fusion recombinant proteins were purified on glutathione-Sepharose 4B (GE Healthcare, Buckinghamshire, United Kingdom) and then eluted in 40 μl of phosphate-buffered saline (PBS) containing 5 U of AcTEV protease (Life Technologies) in order to cleave the GST tag from the protein. Biotinylated NS5A proteins were synthesized from DNA templates by using the cell-free BirA system (44). Biotinylated NS5A proteins (40 μl) were coupled on 15 μl of streptavidin Magnesphere Paramagnetics particles (Promega, Madison, WI) and were dephosphorylated by using 10 U of lambda protein phosphatase (New England BioLabs, Ipswich, MA). After washing three times, protein-coupled beads were incubated with 1 μl of purified recombinant kinases at 37°C for 30 min in 15 μl kinase buffer (50 mM Tris-HCl [pH 7.6], 500 mM potassium acetate, 50 mM $MgCl_2$, and 0.5 mM dithiothreitol) containing 1 μCi of [γ-^{32}P]ATP. After the reaction, the beads were washed twice with PBS and then boiled in sample buffer and separated by SDS-PAGE. Phosphorylated NS5A proteins were visualized via autoradiography, and the relative kinase activity of each kinase was determined by normalizing the band intensity of NS5A to that of NS5A incubated with dihydrofolate reductase (DHFR). The band intensities were quantified using Image J software.

Preparation of viral stocks and virus infections. Cell culture-derived infectious HCV particles (HCVcc) were prepared as described previously (30, 36). HCVpp consisting of HCV envelope glycoproteins, the murine leukemia virus Gag-Pol core proteins, and the luciferase transfer vector and pseudoparticles with the vesiclar stomatitis virus G glycoprotein (VSV-Gpp) were generated in accordance with methods described previously (36, 45). Cells seeded onto 24-well plates were transfected with siRNA and/or plasmid DNA as described below and infected with HCVcc for 4 h at a multiplicity of infection (MOI) of 0.5 to 5 or with diluted supernatant containing HCVpp or VSV-Gpp for 3 h. After infection, the cells were washed with PBS and incubated in fresh complete growth medium for 72 h at 37°C until harvest.

siRNA and plasmid DNA transfections. siRNAs were purchased from Sigma-Aldrich. The sequences were as follows: CKI-α, 5′-GGCUAAAGG CUGCAACAAAdTdT-3′ and 5′-UUUGUUGCAGCCUUUAGCCdTdT-3′; CKI-γ1, 5′-GAGAUGAUUUGGAAGCCCUdTdT-3′ and 5′-AGGGC UUCCAAAUCAUCUCdTdT-3′; CKI-γ2, 5′-GCGAGAACUUCCCAGA GGAdTdT-3′ and 5′-UCCUCUGGGAAGUUCUCGCdTdT-3′; CKI-γ3, 5′-CUUACAGGAACAGCUAGAUdTdT-3′ and 5′-AUCUAGCUGU UCCUGUAAGdTdT-3′; CKI-ε, 5′-GCGACUACAACGUGAUGGUdTd T-3′ and 5′-ACCAUCACGUUGUAGUCGCdTdT-3′; CKII-α′, 5′-CCU AGAUCUUCUGGACAAAdTdT-3′ and 5′-UUUGUCCAGAAGAUCU AGGdTdT-3′; PKACβ, 5′-CAAAUAGAGCAUACUUUGAdTdT-3′ and 5′-UCAAAGUAUGCUCUAUUUGdTdT-3′; Plk1, 5′-GUCUCAAGGC CUCCUAAUAdTdT-3′ and 5′-UAUUAGGAGGCCUUGAGACdTdT-3′; TSSK2, 5′-CACCUACUGACUUUGUGGAdTdT-3′ and 5′-UCCAC AAAGUCAGUAGGUGdTdT-3′; ApoE, 5′-GGAGUUGAAGGCCUACA AAdTdT-3′ and 5′-UUUGUAGGCCUUCAACUCCdTdT-3′; CLDN1, 5′-CAGUCAAUGCCAGGUACGAdTdT-3′ and 5′-UCGUACCUGGCA UUGACUGdTdT-3′; PI4K-IIIα, 5′-CCCUAAAGGCGACGAGAGAdTd T-3′ and 5′-UCUCUCGUCGCCUUUAGGGdTdT-3′. The Mission siRNA universal negative control (Sigma-Aldrich), which is designed to have no homology to known gene sequences, was used as a negative control. Silencer Cy3-labeled GAPDH siRNA (Life Technologies) was used to confirm siRNA delivery efficiency. Basically, 10 nM siRNAs were transfected into cells by using Lipofectamine RNAiMax (Life Technologies) according to the manufacturer's recommended procedures. Plk1 siRNA was transfected at 5 nM because of its cytotoxic effect. Plasmid DNA transfection was carried out by using TransIT-LT1 transfection reagent (Mirus, Madison, WI) according to the manufacturer's protocol. For cotransfection of siRNA and plasmid DNA, 6 pmol of siRNA and 200 ng of plasmid DNA were transfected into Huh7.5.1 cells seeded onto a 24-well cell culture plate by using Lipofectamine 2000 (Life Technologies) according to the manufacturer's instructions.

RNA synthesis and electroporation. HCV RNA synthesis and electroporation were basically performed as described previously (8). In the context of coelectroporation of siRNA and an *in vitro*-synthesized subgenomic reporter replicon, or full-length HCV RNA, a total of 3×10^6 to 5×10^6 Huh-7 cells were electroporated with 120 pmol siRNA and 3 μg SGR-JFH1/Luc RNA or 5 μg JFH-1 RNA at 260 V and 950 μF. After electroporation, the cells were immediately transferred onto 24-well or 6-well culture plates or 10-cm cell culture dishes.

Luciferase assay. Cells harboring a subgenomic reporter replicon and HCVpp-infected cells were lysed in passive lysis buffer (Promega). The luciferase activity was determined using a luciferase assay system (Promega) as previously described (46). Secreted GLuc activity was measured in 25-μl aliquots of cell culture supernatants by using the BioLux *Gaussia* luciferase assay kit (New England BioLabs) according to the manufacturer's recommended protocol. The luminescence signal was measured on an Infinite M200 microplate reader (Tecan, Männedorf, Switzerland).

Quantification of HCV core. HCV core protein in cell lysates and culture supernatants was quantified by using a highly sensitive enzyme immunoassay as described previously (8).

RNA extraction and RT-qPCR. Total cellular RNA was extracted with TRIzol reagent (Life Technologies) according to the manufacturer's instructions. Quantification of cellular gene expression was performed by reverse transcription-quantitative PCR (RT-qPCR) using an Applied Biosystems 7500 fast real-time PCR system (Life Technologies) as described previously (47, 48). Primer/probe sets for qPCR targeting CKI-γ1, CKI-γ2, CKI-γ3, and TSSK2 genes were selected from validated Assays-on-Demand products (Life Technologies).

Intra- and extracellular infectivity assays. Intra- and extracellular infectivities of HCVcc were determined as described previously (8). The infectious titers were expressed as focus-forming units (FFU)/ml.

Cell viability assay. Cell viability was determined using the CellTiter-Glo luminescent cell viability assay (Promega) according to the manufacturer's instructions.

Expression of HCV proteins based on vaccinia virus, immunoprecipitation, immunoblotting, and silver staining. HCV protein expression based on vaccinia virus, immunoprecipitation, and immunoblotting were performed as previously described (8). pJFH1 was transfected into

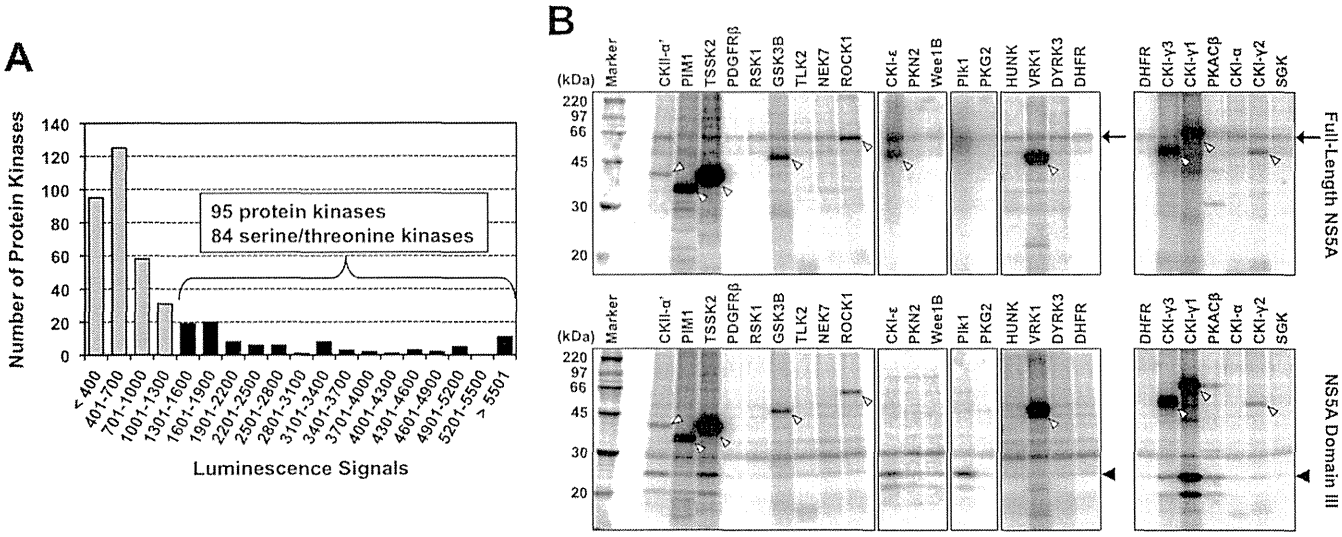

FIG 1 Identification of NS5A-associated kinases. (A) AlphaScreen-based protein-protein interaction assay. FLAG-tagged full-length NS5A, and each of 404 biotinylated human protein kinases, which were synthesized in a cell-free protein production system, were mixed with the detection mixture containing anti-FLAG antibody, protein A-conjugated acceptor beads, and streptavidin-coated donor beads in 384-well plates. Luminescence signals from the mixture were detected. Ninety-five protein kinases were identified with luminescence signals of ≥1,300, of which 84 were serine/threonine kinases. The assay was performed in duplicate for each sample, and data shown are mean values of duplicate experiments. (B) Exemplary autoradiographic images of NS5A phosphorylated *in vitro*. Purified kinases were mixed with biotinylated NS5A proteins coupled on streptavidin beads in kinase buffer containing [γ-^{32}P]ATP. After the reaction, samples were subjected to SDS-PAGE and autoradiography. The arrows, black arrowheads, and white arrowheads indicate phosphorylated full-length NS5A, phosphorylated NS5A domain III, and autophosphorylated kinases, respectively.

cells before infection with vaccinia virus expressing the T7 RNA polymerase. NS5A p58 and p56 protein levels were quantified by densitometry using Image J software. Silver staining of proteins in polyacrylamide gels was carried out using a Silver Stain MS kit (Wako Pure Chemical Industries, Osaka, Japan) in accordance with the manufacturer's protocol.

Subcellular fractionation analysis. Cells were suspended in homogenization buffer (10 mM HEPES-NaOH [pH 7.4], 0.25 M sucrose, and 1 mM EDTA) and disrupted by repeated passages through a 25-gauge needle. After low-speed centrifugation, postnuclear supernatants were layered on linear 11-ml iodixanol gradients from 2.5% to 30% and centrifuged at 40,000 rpm for 3 h in an SW41 rotor (Beckman, Fullerton, CA). Thirteen fractions (0.8 ml in each fraction) were collected from the top of the gradient. Each fraction was concentrated by ultrafiltration units with a 10-kDa molecular mass cutoff (Millipore, Bedford, MA), separated by SDS-PAGE, and immunoblotted with antibodies specific for NS5A, calnexin, and GM130.

Indirect immunofluorescence and microscopy analyses. Cells incubated for 3 days after infection with HCVcc of JFH-1 were fixed with 4% paraformaldehyde for 15 min at room temperature. After washing with PBS, the cells were permeabilized with 0.05% Triton X-100 in PBS for 15 min at room temperature and subsequently incubated in PBS containing 10% goat serum for 1 h. The cells were then costained with antibodies against core and NS5A, followed by incubation with fluorescent secondary antibodies. Cells were counterstained with Hoechst 33342 (Sigma-Aldrich) to label nuclei and BODIPY 493/503 (Life Technologies) to label lipid droplets and then mounted in Vectashield (Vector Laboratories, Burlingame, CA). Subcellular localization of HCV proteins was observed on a Leica SP2 AOBS laser scanning confocal microscope (Leica, Wetzlar, Germany). Colocalization of NS5A and LDs or core was evaluated quantitatively by using the intensity correlation analysis of the Image J software. To statistically compare degrees of colocalization, we determined the intensity correlation quotient (ICQ) (49). ICQ values are distributed between −0.5 and +0.5, with a value of ~0 reflecting random staining and values between 0 and +0.5 versus values between 0 and −0.5 indicative of dependent versus segregated immunolabeling, respectively.

Mass spectrometry analysis. Immunoprecipitated NS5A bands were excised from the gels after silver staining and destained, followed by in gel digestion with trypsin in 50 mM ammonium bicarbonate overnight at 30°C. Liquid chromatography-tandem mass spectrometry (LC-MS/MS) analysis was performed on an LTQ Orbitrap Velos hybrid mass spectrometer (Thermo Fisher Scientific, Bremen, Germany) using Xcalibur (version 2.0.7), coupled to an UltiMate 3000 LC system (Dionex LC Packings, Sunnyvale, CA). The Proteome Discoverer software (version 1.3; Thermo Fisher Scientific) was used to generate peak lists from the raw MS data files. The resulting peak lists were subsequently submitted to a Mascot search engine (version 2.4.1; Matrix Science, London, United Kingdom) and compared against the HCV protein sequences in the NCBI nonredundant protein database (version 20 January 2013; 74,0475 sequences) to identify peptides. The Mascot search parameters were as follows: two missed cleavages permitted in the trypsin digestion; variable modifications including oxidation of methionine, propionamidation of cysteine, and phosphorylation of serine, threonine, and tyrosine; peptide mass tolerance of ±5 ppm; fragment mass tolerance of ±0.5 Da. A minimum Mascot peptide score of 25 was set for peptide selection.

Statistical analyses. Statistical analyses were performed using the Student *t* test unless otherwise noted. A P level of <0.05 was considered significant.

RESULTS

A kinome-wide screening of human protein kinases for identification of NS5A-associated kinases. It has been reported that some protein kinases directly or stably associate with HCV NS5A and phosphorylate it *in vitro* (25, 50, 51). To search comprehensively to identify novel NS5A-associated kinases, a kinome-wide screening for interactions of full-length NS5A with human kinases was initially performed. We synthesized 404 human kinases with a wheat germ cell-free protein production system and screened them in terms of their association with NS5A by using a high-throughput assay system based on AlphaScreen technology (Fig. 1A;

TABLE 1 Serine/threonine kinases that exhibited efficient phosphorylation of NS5A

Kinase	LU	Relative kinase activity[a]	
		FL	D3
TSSK2	8,310	4.24	14.94
CKII-α′	5,068	2.30	8.20
Plk1	3,230	2.70	44.65
CKI-γ2	2,602	4.31	3.15
CKI-γ1	2,560	NA	138.69
CKI-γ3	2,218	0.23	52.51
CKI-ε	2,012	7.95	9.48
PKACβ	1,854	0.15	69.54
CKI-α	1,354	4.66	1.00

[a] LU, light units from the AlphaScreen; FL, full-length NS5A; D3, domain III of NS5A. NA, not assessed due to overlap between purified kinases and NS5A on the gel. The relative kinase activity is the fold increase of the *in vitro* activity of each kinase relative to that of DHFR.

see also Table S1 in the supplemental material). Ninety-five proteins were selected as those that possibly bind to NS5A under the cutoff condition of luminescence signals at ≥1,300. Among them, 84 were serine/threonine kinases, and Plk1 and CKII-α′, the catalytic subunit α′ of CKII whose associations with NS5A have been reported (25, 50), were found in the group as signals at 3,230 (Plk1) and 5,068 (CKII-α′). This suggested that our assay system is highly reliable for screening the NS5A-kinase interaction.

In vitro phosphorylation of NS5A by the identified NS5A binding serine/threonine was determined. Each kinase that was synthesized *in vitro* and purified was incubated with either full-length NS5A or domain III of NS5A in the presence of [γ-^{32}P]ATP and separated by SDS-PAGE. Phosphorylated NS5A proteins were then visualized by autoradiography (Fig. 1B). The relative kinase activity was determined by normalizing the band intensity of phosphorylated NS5A with that of NS5A incubated with DHFR, which had no kinase activity and was used as a negative control. Twenty-nine out of 84 serine/threonine kinases were not accurately assessed due to their low levels of expression. As shown in Table 1, among a total of 55 kinases tested (see Table S2 in the supplemental material), nine (CKI-α, CKI-γ1, CKI-γ2, CKI-γ3, CKI-ε, CKII-α′, PKACβ, Plk1, and TSSK2) exhibited efficient phosphorylation of NS5A, defined as a more-than-4-fold or 8-fold increase in activity against the full-length NS5A or domain III of NS5A, respectively, compared to the negative control. Consistent with previous reports (9, 25, 50), Plk1 and CKII-α′ showed apparent kinase activities against NS5A *in vitro*.

Identification of an NS5A-associated kinase, CKI-α, that is important for the HCV life cycle. On the basis of the *in vitro* screenings, nine candidate kinases were further tested as to whether they play roles in the HCV life cycle. We conducted siRNA-based gene silencing of each kinase and assessed its effect on virion production. Huh7.5.1 cells were transfected with siRNAs targeting the kinases and infected with JFH-1 virus at an MOI of 1, 48 h after siRNA transfection. After an additional 72-h incubation, the viral core levels and infectious virus yields in cell culture supernatants were determined. Knockdown efficiencies of the targeted genes at 72 h after JFH-1 infection are shown in Fig. 2A. Efficient knockdown was confirmed either by immunoblotting or RT-qPCR. Figure 2B indicates the effects of gene silencing on virus production (upper panel) and on cell viability by ATP-based luminescence assays (lower panel). An approximately 30-fold reduction in infectious virus yields was observed following knockdown of ApoE, which has been shown to have important roles in HCV assembly and release (52). Among the kinases tested, silencing of CKI-α showed the most profound inhibition of infectious HCV production (~40-fold) without cytotoxicity. Knock down of CKII-α′ and PKACβ led to a moderate reduction in infectious virus pro-

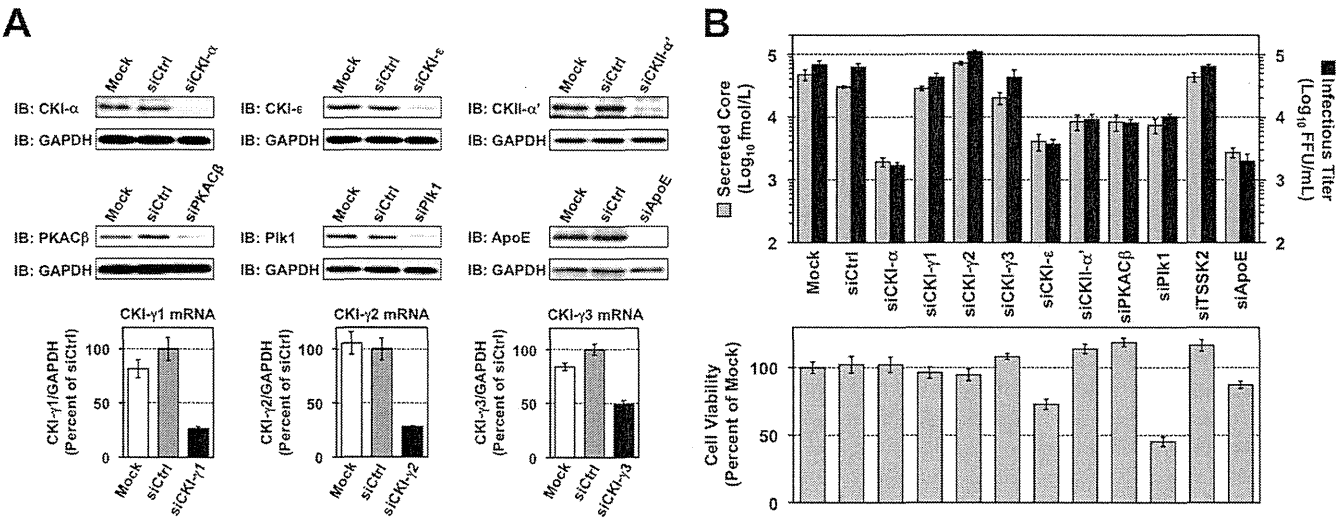

FIG 2 Identification of NS5A-associated kinases involved in the HCV life cycle. (A) siRNA-based gene silencing of NS5A-associated kinases. Huh7.5.1 cells were transfected with siRNAs targeting the indicated genes and were harvested 5 days later for immunoblotting (IB) and RT-qPCR to confirm knockdown efficiencies. mRNA levels of target genes relative to GAPDH mRNA were normalized with values for transfection of control siRNAs (siCtrl), which were set at 100%. Results represent the means ± standard deviations from three independent transfections of siRNA. Mock represents transfection without siRNA. (B) Infectious HCV production and cell viability following knockdown of NS5A-associated kinases. Huh7.5.1 cells were infected with JFH-1 virus at an MOI of 1, 2 days after siRNA transfection. Culture supernatants and cells were harvested 3 days later to determine infectious virus yields (upper panel) and cell viability (lower panel), respectively. Cell viability for each transfection was normalized to that for mock transfection (mock), which was set at 100%. Results shown represent the means ± standard deviations from three independent transfections of siRNA. Mock, transfection without siRNA.

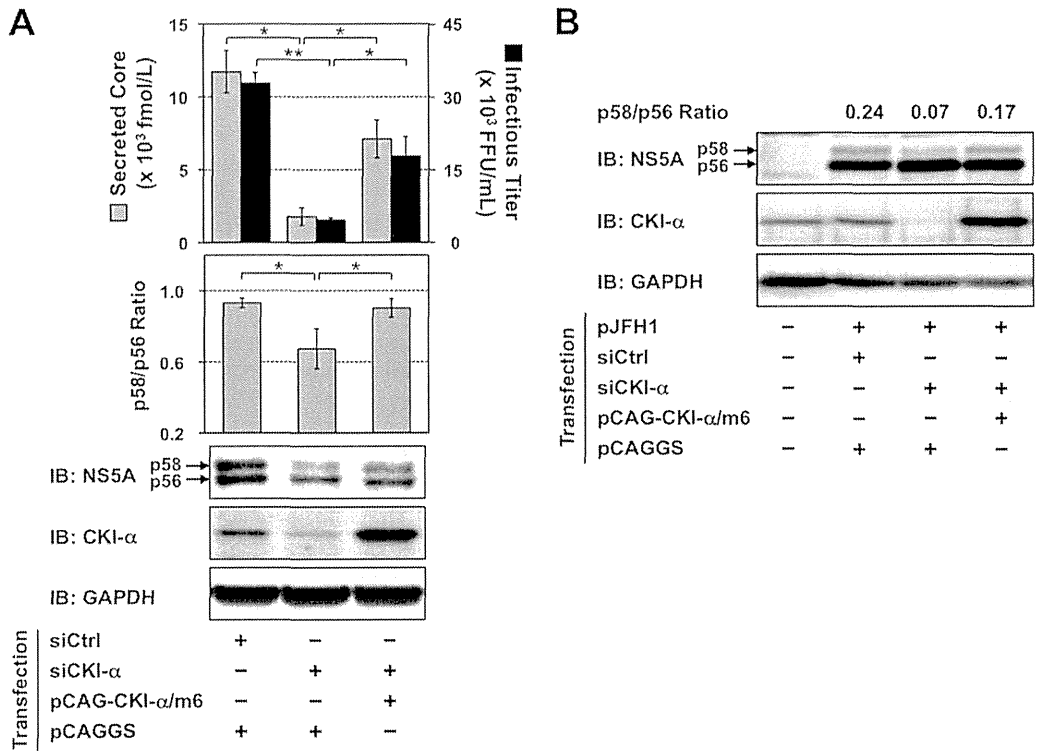

FIG 3 Restoration of NS5A hyperphosphorylation and infectious virus yields by ectopic expression of siRNA-resistant CKI-α. (A) Huh7.5.1 cells were cotransfected with the indicated siRNAs and plasmid DNAs. The next day, cells were infected with JFH-1 virus at an MOI of 0.5. Culture supernatants and cells were harvested an additional 3 days later for measurement of virus yields and immunoblotting (IB). The p58/p56 ratios were calculated after quantifying the band intensities of NS5A. Values shown represent the means ± standard deviations from three replicate experiments. *, $P < 0.05$; **, $P < 0.01$. (B) Huh-7 cells were transfected either with CKI-α siRNA (siCKI-α) or with an irrelevant control siRNA (siCtrl). The next day, cells were retransfected with pJFH1 and pCAG-CKI-α/m6 or empty vector (pCAGGS), followed by infection with vaccinia virus expressing the T7 RNA polymerase at an MOI of 10. NS5A bands were quantified by densitometric analysis, and the p58/p56 ratios were calculated. Immunoblotting images and values shown are representative of two independent experiments.

duction (~10-fold), which was consistent with previous reports showing that CKII-α′ and PKA are involved in virion assembly and viral entry, respectively (9, 53). Knockdown of CKI-ε and Plk1 also resulted in a moderate decrease in virion production (~20-fold), but they induced moderate to severe cell toxicity as well.

Thus, CKI-α, which phosphorylates NS5A, had the highest impact on HCV production based on *in vitro* comprehensive screenings for protein kinases and a subsequent siRNA-based assay.

To further demonstrate that impaired virus production results specifically from CKI-α silencing and is not an off-target effect of the siRNA, cells were cotransfected with CKI-α siRNA and a mutated CKI-α expression vector (pCAG-CKI-α/m6) that contained 6 base mismatches within the site targeted by the CKI-α siRNA without a change in amino acids, followed by JFH-1 infection at an MOI of 0.5 on the next day. The cells and culture supernatants were harvested 3 days later for immunoblotting and titrations of virus yields, respectively (Fig. 3A). Transfection of the CKI-α siRNA led to a significant reduction in infectious virus yields and in the p58/p56 ratio of NS5A. Ectopic expression of the siRNA-resistant CKI-α/m6 apparently restored virus yields ($P < 0.05$), as well as the p58/p56 ratio of NS5A ($P < 0.05$). Similar results regarding the p58/p56 ratio were obtained from immunoblot analysis following vaccinia virus-T7 polymerase-mediated expression of HCV proteins (Fig. 3B). These results indicated that impaired virion production and reduced NS5A hyperphosphorylation are specifically caused by CKI-α silencing. Infectious virus yields showed a closer correlation with the p58/p56 ratio of NS5A than did the expression level of CKI-α, suggesting that the involvement of CKI-α in HCV production is through hyperphosphorylation of NS5A.

CKI-α is mainly involved in virion assembly in the HCV life cycle. Although it has been reported that CKI-α plays roles in the regulation of HCV RNA replication through NS5A phosphorylation, experiments addressing its involvement in the viral life cycle have been performed using the subgenomic replicon system (27). To determine the basic role of CKI-α in the production of infectious HCV, the effect of CKI-α silencing on individual steps in the HCV life cycle was assessed.

First, we used an HCVpp system to analyze viral entry. Two days after the siRNA transfection, the cells were infected with HCVpp derived from JFH-1 or VSV-Gpp and were cultured for a further 3 days (Fig. 4A). Consistent with a previous report (54), CLDN1 knockdown inhibited HCVpp entry by approximately 70%, but not VSV-Gpp entry, compared to transfection with negative control siRNA. CKI-α silencing did not affect HCVpp or VSV-Gpp entry, suggesting that CKI-α is not required for HCV entry.

Second, the effect of CKI-α knockdown was tested using an HCV subgenomic replicon system. Three days after the siRNA transfection, the cells were coelectroporated with the identical siRNA and JFH-1 subgenomic luciferase reporter replicon RNA,